Biochemistry

pubs.acs.org/biochemistry Article

Human γS-Crystallin–Copper Binding Helps Buffer against Aggregation Caused by Oxidative Damage

Kyle W. Roskamp, Sana Azim, Günther Kassier, Brenna Norton-Baker, Marc A. Sprague-Piercy, R. J. Dwyane Miller, and Rachel W. Martin*

Cite This: *Biochemistry* 2020, 59, 2371–2385 Read Online

ACCESS | Metrics & More | Article Recommendations | Supporting Information

ABSTRACT: Divalent metal cations can play a role in protein aggregation diseases, including cataract. Here we compare the aggregation of human γS-crystallin, a key structural protein of the eye lens, via mutagenesis, ultraviolet light damage, and the addition of metal ions. All three aggregation pathways result in globular, amorphous-looking structures that do not elongate into fibers. We also investigate the molecular mechanism underlying copper(II)-induced aggregation. This work was motivated by the observation that zinc(II)-induced aggregation of γS-crystallin is driven by intermolecular bridging of solvent-accessible cysteine residues, while in contrast, copper(II)-induced aggregation of this protein is exacerbated by the removal of solvent-accessible cysteines via mutation. Here we find that copper(II)-induced aggregation results from a complex mechanism involving multiple interactions with the protein. The initial protein–metal interactions result in the reduction of Cu(II) to Cu(I) with concomitant oxidation of γS-crystallin. In addition to the intermolecular disulfides that represent a starting point for aggregation, intramolecular disulfides also occur in the cysteine loop, a region of the N-terminal domain that was previously found to mediate the early stages of cataract formation. This previously unobserved ability of γS-crystallin to transfer disulfides intramolecularly suggests that it may serve as an oxidation sink for the lens after glutathione levels have become depleted during aging. γS-Crystallin thus serves as the last line of defense against oxidation in the eye lens, a result that underscores the chemical functionality of this protein, which is generally considered to play a purely structural role.

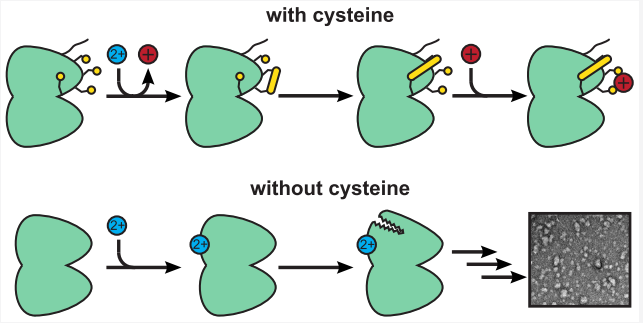

The eye lens is a unique organ due to its optical transparency and minimal metabolic activity. Lens tissue is characterized by high protein concentrations, ranging upward of 400 mg/mL in humans.[1] Ninety percent of lens proteins belong to the α-, β-, and γ-crystallin families. The α-crystallins are small heat-shock proteins that function as holdase chaperones, whereas the β- and γ-crystallins are structural proteins that have evolved for high refractivity and fluorescence quenching. Both β- and γ-crystallins contain two domains connected via a linker sequence and held tightly together by a hydrophobic interface. Each domain contains a double Greek-key motif in which two sets of four antiparallel β-strands create a β-sandwich structure. Even small disruptions to this highly stable structure can lead to stabilization of aggregation-prone intermediates, and ultimately to aggregation.[2−4]

The lens crystallins are extremely long-lived proteins (ELLPs) that face considerable challenges to their stability and solubility. Under a thin exterior layer of epithelial cells, the lens is made of elongated fiber cells that enucleate and lose their organelles during maturation to eliminate light scattering. This process removes the cellular machinery necessary for protein turnover; thus, lens proteins are not replaced during an organism's lifetime. The lens is routinely exposed to ultraviolet (UV) radiation, which can cause structural damage, and the α-crystallins that help maintain solubility can only solubilize damaged structural crystallins and are unable to refold them.[5,6] Consequently, the β- and γ-crystallins have evolved efficient fluorescence quenching mechanisms through conserved structural features and FRET interactions between the buried tryptophans in each domain.[7−10] The aggregation-promoting effect of mutating these Trp residues to Phe is especially strong for those that are most strongly quenched, consistent with the photoprotective quenching requiring multiple Trp residues.[11] Trp residues are also susceptible to undergoing UV photochemistry, producing kynurenine, a small molecule that can act as a UV filter,[12] but can also covalently attach to crystallin proteins, exacerbating oxidative damage.[13] The modified Trp

Received: April 10, 2020
Revised: June 7, 2020
Published: June 8, 2020

https://dx.doi.org/10.1021/acs.biochem.0c00293
Biochemistry 2020, 59, 2371–2385

residue left behind upon kynurenine formation can also promote aggregation, as demonstrated by investigating the properties of point variants mimicking this modification.[14]

The lens environment also contains high levels of glutathione and other antioxidants that serve as redox buffers.[15] Despite these adaptations, deleterious post-translational modifications (PTMs) do accumulate over time.[16,17] An array of PTMs observed in both the soluble and insoluble fractions of aged lenses appear to promote protein aggregation, leading to age-related cataract formation.[18,19] In many cases, the molecular-level details of how PTMs exacerbate aggregation remain unclear. Two modifications of significant interest are deamidation and oxidation. Deamidation, the most commonly observed modification,[17,20] can lead to altered dynamics and reduced stability[21,22] and may occur in parallel with racemization or isomerization.[23,24] Oxidation is arguably the second most common PTM and is thought to accumulate with age as lens antioxidant levels decrease. Mass spectrometric identification of aged lens γ-crystallins has provided evidence for oxidative damage to numerous residues, focally methionine, histidine, tryptophan, and cysteine.[16,25] Reactive oxygen species (ROS) formation in the lens can result from regular exposure to UVA[26] (0.116−0.99 mW cm^{-1}) and UVB (1.2−4.4 × 10^{-4} mW cm^{-1}) radiation, where the ranges represent 2−17% impingement of solar radiation in summer at 40°N applied to data for UVB (295−315 nm) and UVA (315−400 nm) light.[27] However, their formation may also be catalyzed by metal ions found in the lens.

Copper and zinc ions in the lens serve as cofactors for the chaperone α-crystallins but are released upon substrate binding.[28] Whether this release contributes to a negative feedback cycle is currently unknown; however, elevated copper levels have been reported in cataract lenses.[29−31] An increased copper concentration in the lens may also be a feature of diabetes[32] and smoking,[33] but this is difficult to measure directly. Although the concentration of lens Zn^{2+} is several times higher than that of Cu^{2+},[34] copper ions readily produce ROS and induce γ-crystallin aggregation at lower equivalencies.[35] The molecular mechanisms of aggregation due to copper ions and associated ROS are poorly understood but are potentially relevant in other protein aggregation diseases such as Alzheimer's, Parkinson's, and Huntington's.[36,37] The specific interactions with copper ions depend on the structure and function of the protein. Some disease-related proteins like α-synuclein,[38,39] β-amyloid,[40,41] and ubiquitin[42] aggregate in the presence of copper ions, whereas in prion[43] and tau,[44] aggregation is inhibited.

γS-Crystallin is highly expressed in the lens epithelial and cortical fiber cells,[45] while γC and γD, the other highly expressed γ-crystallins, are primarily concentrated in the lens nucleus.[46,47] Because copper ions are relatively evenly distributed throughout the lens,[48] their interactions with all of the structural crystallins are physiologically relevant. We previously reported that divalent cations of zinc, nickel, and cobalt drive γS-crystallin aggregation through intermolecular bridging via cysteines, whereas copper-induced aggregation occurs even in the absence of solvent-accessible cysteines.[35] Solution-state nuclear magnetic resonance (NMR) studies of γD-crystallin suggest that the strongest copper interactions occur at sites with at least two proximal cysteines or histidines.[49] Here we focus on investigating the mechanistic pathways of copper-mediated aggregation of γS-crystallin, which contains a unique cysteine tetrad.[50]

Three of the cysteines, C23, C25, and C27, are solvent-accessible and within disulfide bonding distance of one another. The fourth cysteine, C83, is located on an adjacent β-strand, within disulfide bonding distance of C23 and C27. Although no function is yet known for this tetrad, other γ-crystallins have been observed to have an oxidoreductase-like property where intramolecular disulfides are transferred between proteins.[51] It has been proposed that continual transfers among the highly concentrated γ-crystallins may act as a final redox buffer. A diffusion barrier at the boundary between the lens nucleus and cortex impedes the transport of gluathione into the nucleus,[52] raising the possibility that proteins in the cortex remain reduced longer. However, given the low rate of protein turnover in this environment, oxidation and associated post-translational modifications are inevitable consequences of aging for all of the lens proteins. Because the cysteines of γS are the most solvent-exposed and highest-density cysteines in the γ-crystallin, they may serve as a sink for any disulfide transfer mechanism in the lens.

To better understand the aggregation pathways of γS-crystallin, we have investigated copper(II)-mediated aggregation alongside UV-induced aggregation and point mutations implicated in hereditary cataract. Although the morphologies of all γS-crystallin aggregates examined here are indistinguishable, their relative hydrophobic surface exposures vary. Copper-induced aggregation itself is buffered by the solvent-accessible cysteine residues and is partly reversible through the chelation of copper ions. Aggregation of γS-crystallin can be attributed to copper ion binding and oxidation, which further results in structural changes in the protein. Unsurprisingly, the process of Cu^{2+}-induced aggregation involves several mechanisms; however, the ability of γS to limit oxidative damage further suggests that the lens γ-crystallins have evolved to act as a final redox buffer in the lens.

MATERIALS AND METHODS

Protein Expression and Purification. The human γS-crystallin variants γS-G18V, γS-D26G, γS-V42M, and γS-C23S-C25S-C27S-C115S (γS-C_0) were made using site-directed mutagenesis of the wild-type (γS-WT) construct containing an N-terminal six-His tag and a TEV cleavage sequence (ENLFQG), which leaves a glycine in place of the initiator methionine. The genes encoding each protein were cloned into a pET28a(+) vector (Novagen, Darmstadt, Germany) and overexpressed in a Rosetta *Escherichia coli* cell line (DE3) using Studier's autoinduction protocol.[53] Cell pellets were collected via centrifugation at 4000 rpm for 30 min, resuspended, lysed via sonication, and respun at 14000 rpm for 60 min. Each protein was purified via nickel affinity chromatography, digestion with TEV protease (produced in house), subsequent nickel affinity chromatography to remove the His tag, and, finally, two separate size exclusion chromatography (SEC) runs on a GE Superdex 75 10/300 column (GE Healthcare, Pittsburgh, PA) to ensure pure monomeric protein. All samples were dialyzed into 10 mM HEPES and 50 mM NaCl (pH 7) unless otherwise stated. Prior to measurement, proteins were reduced using 5 mM fresh dithiothreitol (DTT) and dialyzed. Analytical size exclusion of copper-treated samples was assessed using a GE Superdex 75 Increase 10/300 GL column (GE Healthcare).

UVA-Induced Aggregation. Protein solutions at 6 mg/mL (2.5 mL) or 100 mg/mL (1.5 mL) were irradiated with 355 nm light generated using a 10 Hz Nd:YAG laser

https://dx.doi.org/10.1021/acs.biochem.0c00293
Biochemistry 2020, 59, 2371−2385

(Continuum Surelite II, Surelite, San Jose, CA) coupled to a Surelite Separation Package (SSP) 2A (Surelite) to change the pump laser wavelength (1064 nm) via third harmonic generation (laser flux of 29 mJ/cm^2 at 10 Hz). The solutions were continuously stirred and kept between 22 and 24 °C using a Quantum Northwest Luma 40/Eclipse instrument with a Peltier element and recirculator (Quantum Northwest Inc., Liberty Lake, WA). Samples were irradiated for 180 min, which is consistent with our previous investigation of UVA-irradiated crystallins.[54]

UVB-Induced Aggregation. Aggregation of 6 or 100 mg/mL γS-crystallins via 278 nm UVB radiation was accomplished using two 70 mW light-emitting diodes (LEUVA66H70HF00) at 5 mm distances (120° view angle), yielding a mean power density of 58 mW/cm^2. Samples used for transmission electron microscopy (TEM) and FTIR measurements were irradiated for 30 min as preliminary tests showed that this was the shortest exposure time that provided a sufficient amount of aggregated material. TEM images of samples measured at all time points showed morphologically similar aggregates.

Absorbance. Resolubilization assays were performed by adding 200 μL of $CuCl_2$ stock solutions to 200 μL of protein to achieve final solutions of 50 μM protein with varying molar equivalents of $CuCl_2$. Samples were incubated at 25 °C for 8 h and then left at 4 °C overnight prior to measurement. Samples were then spun at 6000 rpm for 20 min, and the supernatant was carefully removed so as not to disrupt any pelleted aggregates. Aggregates were resuspended in 400 μL of buffer with 10 mM ethylenediaminetetraacetic acid (EDTA), vortexed, incubated at 37 °C for 30 min, sonicated for 15 min, and respun at 6000 rpm. This procedure was then repeated with the addition of DTT for a final concentration of 5 mM (2 μL of 1 M DTT). EDTA and DTT treatments were also applied to the initial soluble samples following measurements. Absorbances were measured using a NanoDrop2000. Three samples were prepared for each concentration, and each sample was measured in triplicate. Final absorbance values were corrected for dilution.

Tryptophan Fluorescence. All fluorescence measurements were performed using a Varian Cary Eclipse fluorescence spectrophotometer with 5 μM concentrations. The intrinsic tryptophan fluorescence spectra of protein samples were measured via excitation at 295 nm, and emission spectra collected from 310 to 400 nm.

ANS Fluorescence. The fluorescence of 8-anilinonaphthalene-1-sulfonic acid (ANS) was used as an indicator for hydrophobic surface exposure. Samples were prepared at a final concentration of 50 μM with 750 μM ANS (based on prior work[55]) and allowed to incubate at room temperature for 1 h. Fluorescence spectra were measured from 450 to 600 nm with an excitation at 390 nm, using 20 nm slit widths.

Isothermal Titration Calorimetry (ITC). ITC measurements of copper ion binding were performed using a MicroCal PEAQ-ITC instrument (Malvern Instruments, Northampton, MA). Two hundred microliters of freshly reduced γS-WT (135 μM) and S-C_0 were titrated with 4 mM $CuCl_2$ at 25 °C. Injections were made every 225 s, with 25 titrations in total. The ITC data were initially analyzed using MicroCal PEAQ-ITC Analysis Software. The reported parameters are the mean and standard deviation of three independent trials. On the basis of the similarity of the transition metal FRET (tmFRET) and initial ITC binding data, the binding parameters for γS-C_0 were determined first using a single-binding site model. The number of sites was constrained between 0.25 and 1.5, and the binding constant was limited to 1×10^{-8} based on preliminary model fitting performed in R[56] using the 'Ritc' package.[57] For γS-WT, the data were fit to a two-site binding model, using the γS-C_0 parameters and initial values for the second γS-WT binding event.

Fluorescence Quenching. Fluorescence quenching of γS-WT and γS-C_0 was performed by adding 2 μL of 125 μM $CuCl_2$ to 500 μL of 5 μM protein, yielding 0.1 molar equivalent steps. Following the addition of $CuCl_2$, the sample was gently shaken and then allowed to equilibrate for 20 s prior to measurement. The emission spectra were recorded from 320 to 360 nm using 295 nm excitation to minimize tyrosine and phenylalanine absorbance. The Stern−Volmer binding constants were calculated assuming static quenching using the equation $F_0/F = 1 + K_{SV}[Q]$, where F_0/F is the ratio of the initial fluorescence intensity at 330 nm, K_{SV} is the Stern−Volmer binding constant, and [Q] is the concentration of $CuCl_2$. For γS-WT, two separate models were generated to fit the data from amounts less than and greater than 0.5 equiv of $CuCl_2$, as a clear difference in quenching is observed. The K_{SV} of γS-C_0 was calculated through ∼1.5 molar equivalents. After this point, the F_0/F data exhibit logarithmic behavior, consistent with binding saturation in fluorescence quenching studies of proteins containing buried tryptophans.[58,59] In addition, after 1.5 molar equivalents, linear regression models maintain an r^2 of >0.99. No significant changes were observed in the K_{SV} of either protein when calculated for all measured emission wavelengths; therefore, the data presented use the 330 nm emission intensities.

Fourier-Transform Infrared Spectroscopy (FTIR). Aggregates of γS-G18V, γS-D26G, and γS-V42M were collected from samples stored at 5 mg/mL and 4 °C for several weeks. All aggregates and soluble protein were separated via centrifugation and lyophilized. Samples were then resuspended in D_2O for 24 h and lyophilized again. Measurements of all powders were taken using a Jasco FT/IR-4700-ATR-PRO ONE instrument (Jasco, Easton, MD) over the range of 400−4000 cm^{-1} with 4 cm^{-1} resolution. Data from 1700 to 1475 cm^{-1} were normalized to peak amide I band absorbance.

Liquid Chromatography−Mass Spectrometry (LC−MS). In-line separation of protein and peptide fragments and subsequent mass spectrometry measurements were performed on a Waters Xevo XS-QTOF instrument using a Waters BEH C4 50 mm column with a flow rate of 0.3 mL/min. Protein samples were diluted 10:1 in 0.1% formic acid and separated using a gradient in which solvent A was 100% 0.1% formic acid in water and solvent B was acetonitrile. The gradient started at 3% solvent B for 1 min followed by a linear ramp to 27% B over 5 min. Peptide samples were generated from aggregates produced by incubating freshly reduced γS-WT with 1 equiv of $CuCl_2$ for 24 h at room temperature. Protein samples of 1 mL at 200 μM were incubated overnight with 3 μg of trypsin at 37 °C. Samples were diluted and measured in a manner identical to that of protein samples except for an extended separation time of 25 min. Reduced peptide samples were treated with fresh DTT for 5 min at room temperature prior to measurement. All data analysis was performed using BioPharmaLynx software for fragment identification. Peptide fragment identities were confirmed via direct inspection of the raw data and isotope pattern analysis. Over several replicates, the sequence coverage varied between 70% and 85%. For each of the cysteines, at least one fragment was identified. The

https://dx.doi.org/10.1021/acs.biochem.0c00293
Biochemistry 2020, 59, 2371−2385

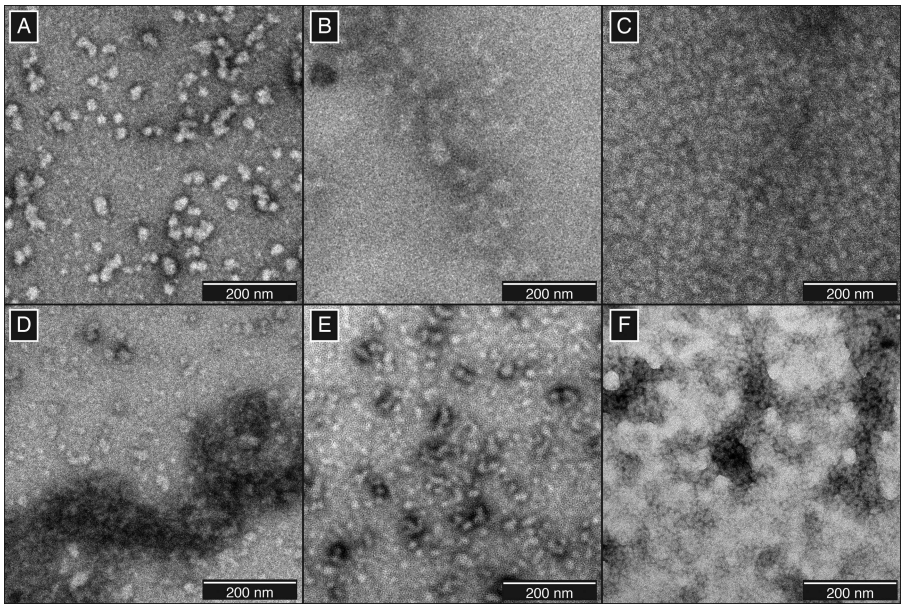

Figure 1. TEM micrographs of γS-crystallin aggregates. (A) Native aggregates of γS-D26G, (B) γS-G18V, and (C) γS-V42M. Photodamaged aggregates formed using (D) UVA or (E) UVB radiation. (F) Aggregates resulting from the treatment of 0.5 equiv of $CuCl_2$.

presence of disulfide-bonded fragments was confirmed via the disappearance of identified peaks in reduced samples.

Sodium Dodecyl Sulfate−Polyacrylamide Gel Electrophoresis (SDS−PAGE). The γS-WT (200 μL total volume, 150 μM) samples were aggregated using 0.1, 0.2, 0.4, 0.6, 0.8, 1, 1.5, 2, 3, or 5 equiv of $CuCl_2$ at 25 °C for 4 h and then left at 4 °C overnight. The samples were then centrifuged, and the supernatant was removed without disturbing the pellet. Prior to loading, 10 μL of protein was mixed with 10 μL of loading dye [62.5 mM Tris-HCl, 2% sodium dodecyl sulfate, 25% glycerol, and 0.01% bromophenyl blue (pH 6.8)], 1 μL of 2-mercaptoethanol, and 1 μL of EDTA (final concentration of 1 mM) and heated at 70 °C for 90 s. Samples were run on a 12% Mini-Protean TGX gel at 115 V for 85 min and stained using Coomassie blue dye. Each gel was run at least twice to verify reproducibility.

Analytical Size Exclusion Chromatography (SEC). Samples of freshly reduced γS-crystallins were mixed with $CuCl_2$ in 1:1 ratios resulting in a final sample at 50 μM with 0, 0.25, 0.5, 0.75, or 1 equiv of $CuCl_2$. The samples were allowed to incubate at room temperature overnight and subsequently stored at 4 °C until use. Prior to measurement, samples were treated with a 100-fold excess of EDTA. For re-reduced samples, subsequent treatment with fresh DTT followed by incubation at 37 °C for 30 min was also performed. Prior to measurement, samples were passed through a 0.45 μm filter to eliminate potential aggregates. The separation of soluble aggregated species was achieved by loading 500 μL of the sample onto a Superdex 75 Increase 10/300 GL column. The sample and column temperatures were maintained at 4 °C, and the flow rate was 0.8 mL/min. Elution was monitored via the absorbance at 280 nm.

Transmission Electron Microscopy (TEM). The morphologies of the γS-crystallin aggregates formed on exposure to acidic buffer, UV irradiation, or metal ion treatment were investigated by TEM. Samples were prepared at a concentration of 6 or 100 mg/mL and used without further dilution. Negatively stained samples for TEM were prepared on commercial carbon-coated 400 mesh copper grids (Plano GmbH, Wetzlar, Germany). The grids were made hydrophilic by glow discharge treatment, whereupon 2 μL of a sample solution was applied and allowed to soak for 45 s before blotting. The grids were then rinsed twice with 50 μL of deionized water, followed by blotting. Negative staining was performed by applying 4 μL of a 1% uranyl acetate solution, followed by immediate blotting. Application of 4 μL of uranyl acetate was then repeated, this time being allowed to soak for 20 s before a final blotting step. TEM micrographs were then recorded in a JEOL JEM 2100 instrument with an accelerating voltage setting of 120 kV.

RESULTS AND DISCUSSION

Amorphous-Looking Aggregates Are Formed from Point Variant, UV-Irradiated, and Copper-Damaged γS-Crystallins. Unlike the amyloid fibrils central to many protein deposition diseases, crystallin aggregates are frequently characterized as amorphous-looking, although fibrillization of lens crystallins is readily induced *in vitro* using extreme pH conditions. Herein, we have investigated the aggregation of wild-type human γS-crystallin (γS-WT) resulting from treatment with copper(II) and compared the aggregates to those resulting from known cataractous point mutations and UV irradiation. TEM was used to image aggregates of γS-G18V, γS-D26G, and γS-V42M that formed after being stored at 4 °C for more than one month (Figure 1A−C), which we will term "native aggregates". For each variant, the native aggregates have a granular appearance and are composed of smaller globular particles roughly 25 nm in diameter on average (Figure S1), similar to those we have previously observed for UV-aggregated γS-crystallin samples.[54] The clustering of smaller, component aggregates that can be observed in each case is similar to that observed for the γD-P23T point variant in prior studies by other groups.[60,61] Furthermore, the morphological similarity of aggregates observed here is striking, as the D26G variant—in which only a surface salt bridge is lost[62]—is qualitatively different from G18V and V42M, both of which cause more substantial structural changes to the N-terminal domain.[63,64]

https://dx.doi.org/10.1021/acs.biochem.0c00293
Biochemistry 2020, 59, 2371−2385

TEM micrographs of γS-crystallin were recorded following UVA and UVB irradiation (Figure 1D,E). Although UVA and UVB can both catalyze ROS formation, the lower levels of UVB reaching the lens are effectively quenched due to their absorption by aromatic residues, particularly the four strongly conserved tryptophans.[8] Irradiation over both wavelength ranges produces aggregates that are similar in size to the point variant aggregates and similarly appear to lack any well-defined morphology that would be consistent with an ordered, repeating structure. To ensure that the UV aggregates formed were representative, we varied the concentration and irradiation times of the samples to assess potential differences. In all cases, once formed, the size and morphology of the observed aggregates did not exhibit any notable differences (Figures S2 and S3). Likewise, photodamaged point variants also show distinct, small component aggregates similar in size to native aggregates (Figure S4).

As observed for point variants and UV-irradiated samples, copper(II)-induced aggregates lacked distinctive repetitive structure (Figure 1F), consistent with observations of copper-(II)-induced aggregates of γD-crystallin.[49] To test for differences that would enable investigation of specific aggregation pathways, we probed the structure of the resulting aggregates via FTIR. In FTIR of proteins, the amide I band largely results from the C═O stretching vibration, while the amide II band represents the N−H bending vibration and C−N stretching vibration.[65] The amide absorption frequencies of protein secondary structures differ from one another; therefore, one can infer structural differences between proteins by comparing their amide I and II bands. Between the soluble and aggregated variant γS-crystallins, minimal differences were observed in the amide I band line shape, suggesting that the overall β-sheet structure is retained for each of the solid aggregates (Figure S5). Likewise, the changes observed following UVB irradiation or treatment with copper ions are also minimal. Interestingly, the absorption of the amide I mode relative to amide II decreases for all aggregates, as well as the soluble UVB- and copper salt-treated species. The extent to which the amide I and amide II peaks are modified for the UVB-treated samples differs noticeably from those observed in the one previous study of structural changes in UV-treated γB-crystallin.[66] We hypothesize that the smaller changes we observe are the result of minor conformational changes; however, specific structural modifications cannot be readily determined via FTIR alone, making this a promising direction for future high-resolution structural studies.

We next turned to potential changes in hydrophobic surface exposure to better understand the effect of copper treatment. Cataract-causing point mutations serve as convenient references, as increased hydrophobic surface exposure can result from mutations within the hydrophobic core[67,68] or on the protein surface,[55,69] although not all aggregation-prone variants exhibit increased hydrophobic surface exposure.[62] We assessed differences in the exposed hydrophobic surface of γS-crystallin following copper and UVB treatment using ANS, a small molecule probe that fluoresces strongly when coordinated to a protein through a combination of electrostatic and hydrophobic interactions.[70] The soluble fraction of γS-WT that remains after $CuCl_2$ treatment has an ANS fluorescence spectrum similar to that of γS-D26G (Figure 2), for which no structural changes are known. Both spectra have fluorescence maxima slightly greater than that of untreated γS-WT. In contrast, the two point variants with known increases in hydrophobic surface exposure, γS-G18V and γS-V42M, show considerable increases in ANS fluorescence intensity upon binding the dye.

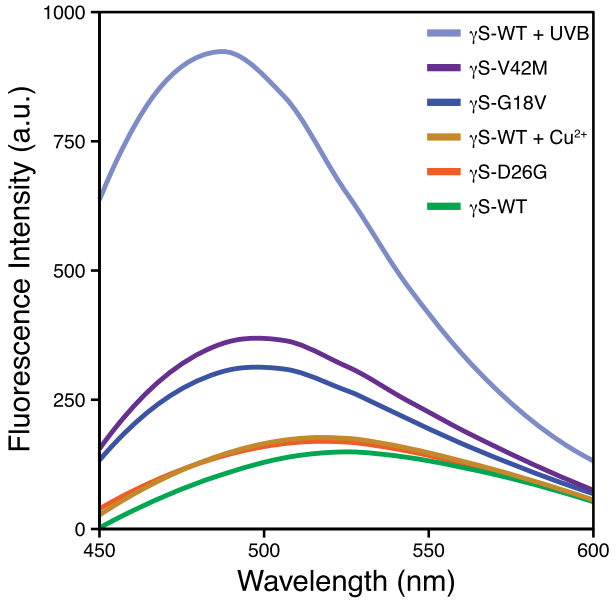

Figure 2. Fluorescence spectra of ANS upon binding to γS-crystallins. In each case, 50 μM soluble protein was incubated with 750 μM ANS to probe changes in hydrophobic surface exposure. UVB irradiation produces considerable hydrophobic exposure. The soluble γS-WT remaining after the addition of $CuCl_2$ exhibits minimal changes in its ANS fluorescence spectrum relative to that of γS-WT. Point variant ANS fluorescence differences are consistent with previous reports.

Interestingly, UVB-exposed γS-WT exhibits the greatest increase in ANS fluorescence, with an intensity more than double that of γS-V42M. UV-induced damage of γ-crystallins primarily occurs via tryptophan, cystine, and methionine oxidation[71] and can disrupt the hydrophobic core of the protein, as all four tryptophans are buried and integral to the Greek-key domain structure. In contrast, given the absence of large-scale unfolding, we hypothesize that copper-mediated damage is limited to binding or oxidation of surface residues. In a prior study, we observed small amounts of methionine and cysteine oxidation at high $CuCl_2$ concentrations, which was part of the rationale for further investigation of the mechanism.[35] Our results indicate that the remaining soluble γS-WT forms following UVB and copper treatment differ in their extent of hydrophobic surface exposure, with aggregation likely occurring through different pathways. We previously observed that γS-WT aggregates from copper treatment contain PTMs, albeit at low levels.[35] Taken together, these data indicate that the binding interactions of copper and γS-crystallin promote the onset of aggregation.

Copper Induces Aggregation via Multiple Mechanisms. Recently, divalent cations of transition metals such as copper,[49,72] zinc,[35,73] and mercury[74] have been shown to facilitate γ-crystallin aggregation. We previously observed that γS-crystallin samples treated with Zn^{2+}, Ni^{2+}, and Co^{2+} aggregate through an intermolecular bridging-type mechanism, which becomes negligible upon the mutation of all solvent-accessible cysteines to serines. Surprisingly, removing these cysteines accelerated copper-induced aggregation.[35] To systematically evaluate the effect of copper ions, we began by investigating the aggregation of γS-WT and the engineered γS-

https://dx.doi.org/10.1021/acs.biochem.0c00293
Biochemistry 2020, 59, 2371−2385

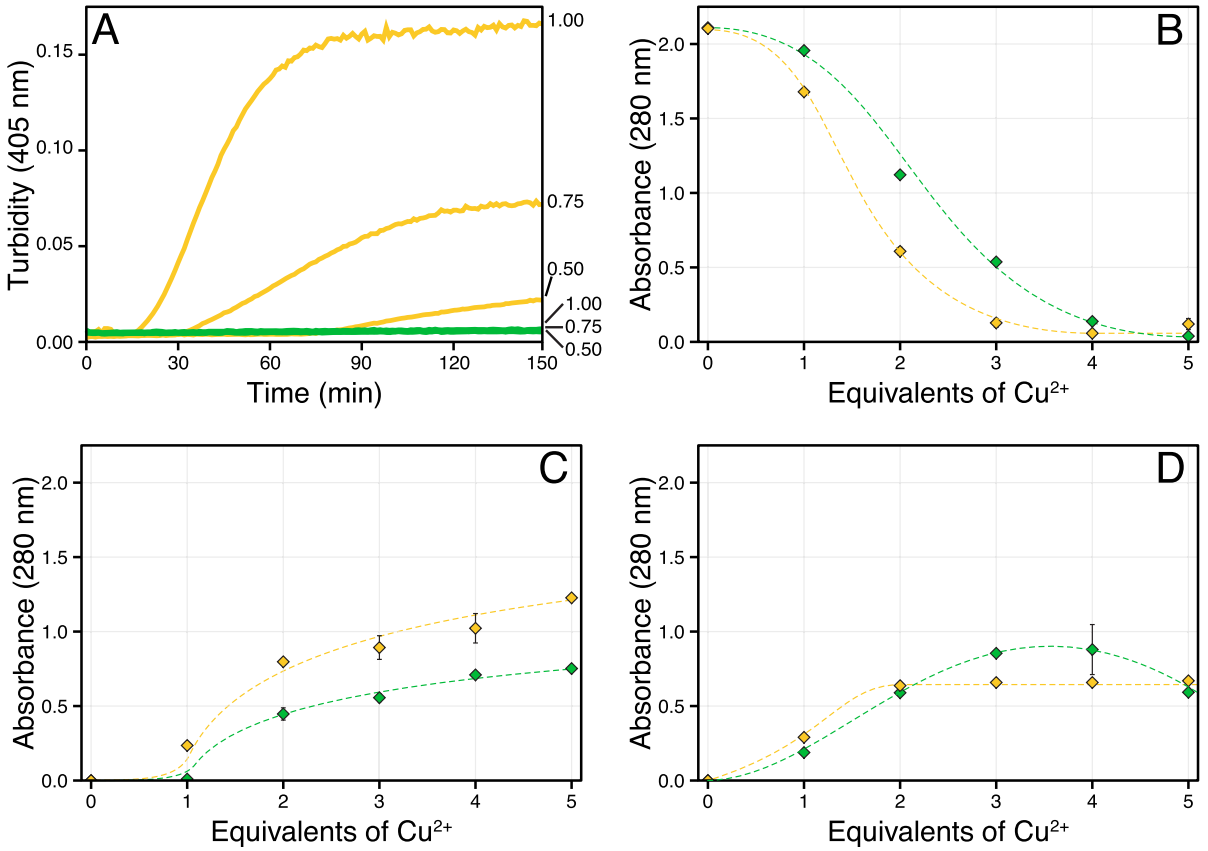

Figure 3. Absorbance at 280 nm of γS-WT (green) and γS-C_0 (gold) measured following the addition of $CuCl_2$. (A) Aggregation kinetics of γS-WT (green) and γS-C_0 (gold) following the addition of 0.5, 0.75, or 1 equiv of $CuCl_2$ (listed at the right). After 150 min, no turbidity was observed for γS-WT, whereas the onset and extent of γS-C_0 turbidity increased with copper concentration. (B) Absorbance of the supernatant following centrifugation. (C) Absorbance of proteins resuspended from copper-induced aggregation via EDTA. (D) Absorbance of proteins resuspended from copper-induced aggregation via DTT. Error bars represent one standard deviation. The lines serve as a visual guide.

C_0 variant, in which all four solvent-accessible cysteines (C23, C25, C27, and C115) were mutated to serine. Consistent with our previous results, γS-WT aggregates to a lesser total extent than γS-C_0 when treated with varying equivalents of $CuCl_2$ (Figure 3A,B). To quantify aggregation-promoting factors, we treated insoluble copper-induced aggregates with excess EDTA (10 mM) to recover protein precipitated through intermolecular bridging. Both proteins show comparable amounts of recovery relative to the amount of insoluble aggregate formed (Figure 3C). Subsequently, we resuspended the remaining aggregates in the presence of DTT (5 mM) to disrupt potential disulfide cross-links contributing to aggregation (Figure 3D). Unexpectedly, we observed apparent resolubilization of both proteins, although small aggregates may still be present. Although intermolecular disulfides or non-native disulfide-trapped folds may play a role in causing aggregation, we suspected that the copper oxidation state may explain the observed behavior. EDTA is an effective Cu(II) chelator (K_d of $10^{-18.8}$ M);[75] however, its ability to abstract Cu(I) is more limited. In comparison, DTT binds Cu(II) strongly and Cu(I) less so[76,77] and is capable of generating Cu(I) from Cu(II). Therefore, DTT resolubilization may proceed via coordination of bound Cu(I) or by reduction of tightly bound Cu(II) to Cu(I), resulting in a more weakly bound ion. Alternatively, protein-bound copper may result in steric shielding, limiting the EDTA to fewer accessible coordination sites, but still allowing for bidentate binding by DTT. In each case, the ability of a second chelating agent to resolubilize aggregates following EDTA treatment suggests that copper ion-induced aggregation occurs though more than one mechanism and may involve binding to at least two sites. In addition to intermolecular bridging and intermolecular disulfide bonding, we hypothesized that the tightly bound copper ions may induce local structural modifications leading to additional aggregation pathways.

Structural changes to the resolubilized proteins were investigated via fluorescence and circular dichroism (CD) spectroscopy (Figure 4.) The tryptophan fluorescence of γ-crystallin is a sensitive measure of conformational changes that can be observed through reduced FRET efficiency and red shifting due to increased polarity in the local tryptophan environment.[7,9] For both proteins, the EDTA-resolubilized species exhibit the greatest extent of red shifting of the fluorescence signal, indicating the most unfolding. The extent of unfolding for all copper-treated species was assessed via the 355 nm/325 nm fluorescence intensity ratio.[78,79] This method is preferable to measuring at a single frequency, as it provides a quantitative measure of unfolding, which is particularly useful for detecting incomplete unfolding, as in the case in which one domain unfolds before the other. The ratio is also useful for comparing samples where different degrees of partial unfolding have occurred.

The fluorescence ratios of EDTA-resolubilized γS-WT and γS-C_0 increased from 0.57 to 0.78 and from 0.59 to 0.96, respectively. The 355 nm/325 nm fluorescence ratios around ~0.9 are indicative of partial domain unfolding. Similar

https://dx.doi.org/10.1021/acs.biochem.0c00293
Biochemistry 2020, 59, 2371−2385

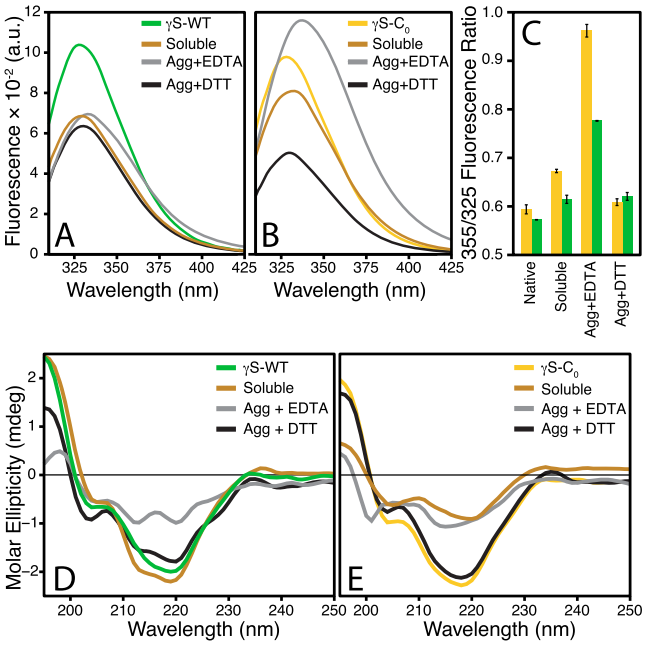

Figure 4. Fluorescence and CD spectra of soluble and aggregated γS-WT and γS-C_0 after incubation with 2 equiv of $CuCl_2$. Both EDTA-resolubilized species exhibit the greatest extent of unfolding, with considerably more unfolding occurring in γS-C_0 than in γS-WT. (A) Fluorescence of untreated and copper-incubated samples of γS-WT. (B) Fluorescence of untreated and copper-incubated samples of γS-C_0. (C) The 355 nm/325 nm fluorescence intensity ratio for each of the samples measured in panels A and B. Error bars represent one standard deviation. (D) CD of untreated and copper-incubated samples of γS-WT. (E) CD of untreated and copper-incubated samples of γS-C_0.

fluorescence ratios have been reported for the chemical denaturation of γS-G18V,[80] γS-S39C,[3] γS-V42M,[67] and γD-V75D.[81] NMR and SAXS of chemically denatured γD-V75D have shown the CTD remains folded while the NTD becomes unfolded.[82] In the case of copper-induced unfolding, we hypothesize that the NTD similarly unfolds. The three NTD cysteines are significantly more solvent-exposed than the lone CTD cysteine and thus likely to interact with copper, leading to structural modifications. Interestingly, the fluorescence ratios for both DTT-resolubilized proteins suggest negligible unfolding, further evidencing that multiple mechanisms are involved in copper-induced aggregation.

The CD spectra were also measured for all copper-treated species to compare to the fluorescence ratio unfolding results. For γS-WT, the CD spectrum exhibits a minimum at 218 nm, indicative of high β-sheet character, consistent with the solution-state NMR structure.[64] Minimal structural changes were evidenced in soluble γS-WT. For soluble γS-C_0, the CD absorbance is low relative to that of the untreated sample and shows an increased absorbance around 205 nm. This result is likely from a minor decrease in the β-sheet character with a concomitant increase in random coil character but is more dramatic than the change observed in the fluorescence ratio. In comparison, the CD spectra for both DTT-resolubilized species exhibit minimal differences relative to those of the untreated protein, indicating only minor structural differences, while the EDTA-resolubilized species of both proteins indicate considerable structural changes. For γS-C_0, the minima near 200 nm and from 212 to 218 nm indicate a considerable decrease in the level of β-sheet character with no changes in the α-helix content and an increase in the random coil content. The CD spectra of EDTA-resolubilized γS-WT are similar but lack the minima near 200 nm, suggesting the structural changes

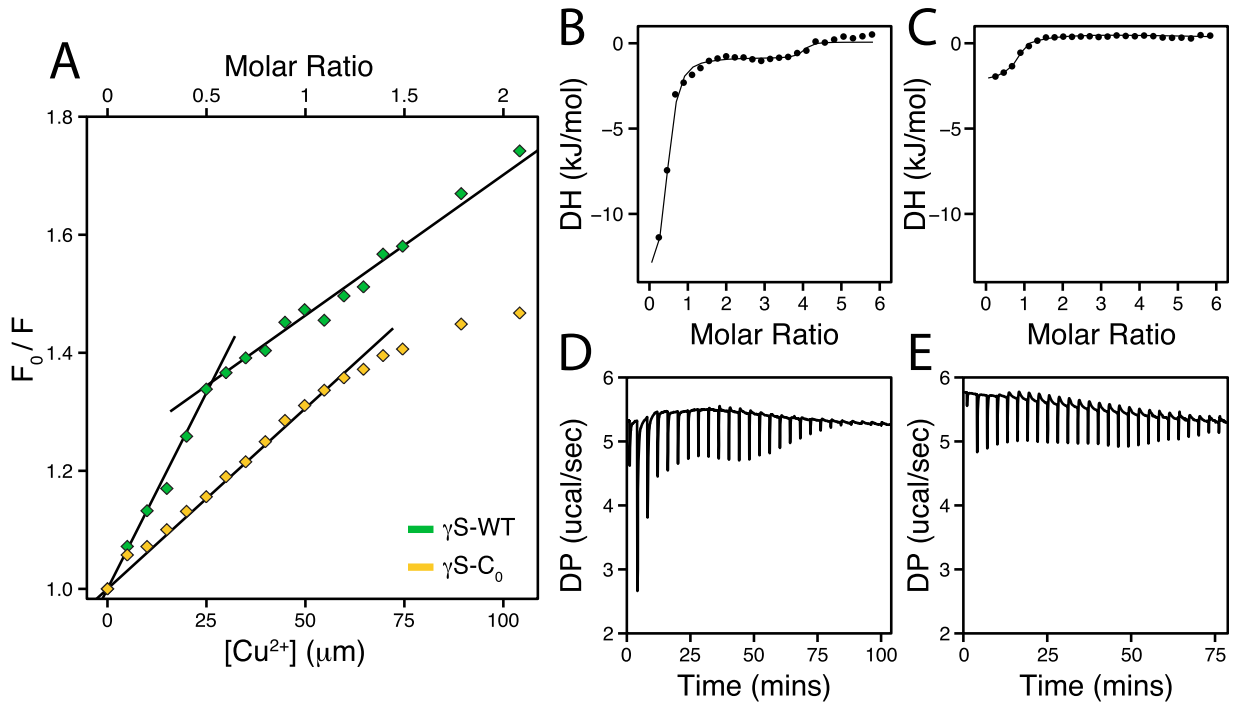

Figure 5. (A) Stern–Volmer plots of the fluorescence quenching for γS-WT (green) and γS-C_0 (gold) resulting from $CuCl_2$ titration. The plotted data show the ratio of the initial fluorescence intensity at 330 nm to the intensity following the addition of $CuCl_2$. The γS-WT data after 0.5 equiv were fit to a second model. Data up to 1.5 equiv were used for γS-C_0. (B and C) Integrated heat and (D and E) raw data from isothermal titration calorimetry measurements of titrations of γS-WT (B and D) and γS-C_0 (C and E) with $CuCl_2$ at 25 °C.

https://dx.doi.org/10.1021/acs.biochem.0c00293
Biochemistry 2020, 59, 2371−2385

are not nearly as severe as those in C_0. These results are consistent with the observed fluorescence ratio data, indicating the extents of unfolding in the EDTA- and DTT-resolubilized species differ considerably. In addition, these observations support a function for the NTD cysteines in preventing copper-induced unfolding.

The Cysteine Loop in γS-WT Is Responsible for High-Affinity Copper Binding. While analyzing the γS-crystallin fluorescence data, we suspected that the reduced intensity of the copper-treated species resulted from transition metal FRET (tmFRET) interactions with bound copper. Although no metal-binding site has previously been identified for human γS-crystallin, several transition metals can drive intermolecular bridging via the cysteine loop.[35] As copper appeared to bind γS at two or more sites, we presumed one to be the cysteine loop. TmFRET interactions can be used to calculate binding constants from fluorescence quenching when the interactions occur between the metal and fluorophore. The observed tmFRET from yS-crystallin is complicated by the presence of four buried tryptophans; therefore, we measured the quenching constants for γS-WT and γS-C_0 to probe how the solvent-accessible cysteines affect copper ion binding.

Stern−Volmer plots and binding constants (K_{SV}) were generated from fluorescence measurements of $CuCl_2$ titrations (Figure 5A). In the Stern−Volmer plot for γS-WT, the ratio of the initial to $CuCl_2$-treated fluorescence intensity—used to measure the extent of quenching—sharply changes at 0.5 equiv of $CuCl_2$. Two K_{SV} values were calculated around this point and show that the strong level of initial binding of γS-WT ($K_{SV1} = 12.1 \times 10^3$) is decreased >2-fold in the second regime ($K_{SV2} = 4.5 \times 10^3$) (Table 1). The K_{SV2} of γS-WT is similar to the K_{SV1} of γS-C_0 (6.1×10^3). We posit that the second copper binding event with γS-WT is equivalent to γS-C_0 binding and occurs following saturation of the cysteine loop. In addition, the binding and subsequent change in behavior at 0.5 equiv of copper for γS-WT is suspected to result from metal bridging between two cysteine loops.

Table 1. Stern−Volmer Binding Constants Determined via tmFRET for γS-Crystallins and $CuCl_2$ at pH 7 and 25 °C[a]

protein	K_{SV1}	K_{SV2}
γS-WT	$(12.1 \pm 1.4) \times 10^3$	$(4.51 \pm 0.4) \times 10^3$
γS-C_0	$(6.11 \pm 0.3) \times 10^3$	

[a]Rows 1 and 2 are different isotherms from the same sample of γS-WT.

Although tmFRET measurements give evidence for clear differences in copper binding by γS-WT and γS-C_0, we were unable to directly calculate binding constants from these data. Therefore, we used isothermal titration calorimetry (ITC) to probe the binding interactions (Figure 5B−D). Consistent with the tmFRET quenching, γS-WT exhibits two binding events and was analyzed using a two-site model. The first γS-WT binding event exhibits an affinity (K_d = 50 μM) that is higher than that of the second (K_d = 4 mM) (Table 2). For γS-C_0, the single binding event is similar in affinity to the second γS-WT binding event, further suggesting that the initial, high-affinity binding occurs at the cysteine loop.

In comparing known copper-binding sites to the cysteine loop, we observed no similar structural motifs, although several copper-transport proteins have similar local concentrations of cysteine residues. The binding sites of these metalloproteins coordinate to Cu(I) with remarkable affinity, $\leq 10^{-21}$ M for CueR,[83] and primarily use linear bicysteinate coordination. We suspect that a similar binding mode may occur for γS-WT, as the C23−C25, C23−C27, and C25−C27 side chain sulfurs (minimized side chain rotamer distances of 3.8 ± 0.5, 3.1 ± 0.3, and 4.3 ± 0.1 Å, respectively[64]) are sufficiently proximal in the 20 lowest-energy NMR confirmations of the native protein. Predictions of binding of Cu(I) to γS-WT generated using MIB[84,85] also highlight the cysteine loop as the most likely binding site (Figure S6).

The calculated binding constant of the first γS event is considerably weaker than those of characterized domains of Atx1,[86] HMA7,[87] WLN5,[76] and other metalloproteins employing cysteinate-binding motifs. As shown for *Pseudomonas aeruginosa* azurin, the thermodynamics of strong Cu(I) and Cu(II) binding are obscured in ITC analysis by side chain deprotonations and metal−buffer interactions.[88] For the γS-WT−copper binding measured here, potential disulfide bond formation and other unknown interactions with the protein may also contribute to the observed binding thermodynamics. Given these considerations, we hypothesize that the affinity of the cysteine loop for Cu(I) may be higher than reported here.

Cation-Mediated Bridging and Disulfide Bonding Are the Primary Modifications Resulting from Copper Treatment of γS-Crystallin. To determine whether the copper-induced structural changes observed at the protein level translate into any higher-order structure, we probed aggregate size distributions via analytical SEC. To probe the smallest component sizes of the γS-WT and γS-C_0 species, all samples were treated with EDTA and DTT prior to separation. The SEC traces of soluble and DTT-resolubilized γS-C_0 are primarily monomeric (Figure S7). This result is consistent with the minimal structural changes observed via CD and fluorescence and supports a copper-induced aggregation mechanism involving metal-bridged cross-linking with coordination to non-cysteine residues. Despite the predominance of monomeric species, soluble and DTT-resolubilized γS-WT, but not γS-C_0, also contain a dimeric peak. As intermolecular disulfides between γS-crystallin are readily reducible, it is plausible that the cysteines are responsible for this alternative dimerization. The 2:1 stoichiometry observed in the binding assay also suggests that copper-mediated dimerization via the cysteine loop may be responsible; however, alternate mechanisms such as a covalent intermolecular bond, e.g., dityrosine,[89] also require further investigation.

The chromatograms of EDTA-resolubilized γS-WT and γS-C_0 show higher-molecular weight species than soluble and

Table 2. Average Thermodynamic Parameters for γS-Crystallins and $CuCl_2$ at pH 7.0 and 25 °C

protein	n	K_{ITC} (M^{-1})	ΔH (kJ/mol)	ΔG (kJ/mol)	$-T\Delta S$ (kJ/mol)
γS-WT	0.38 ± 0.01	$(4.7 \pm 3.8) \times 10^8$	−55.6 ± 6.4	−42.6 ± 1.8	12.9 ± 7.5
γS-WT	3.70 ± 0.20	$(4.0 \pm 4.0) \times 10^6$	−5.1 ± 1.0	−31.8 ± 2.3	−26.7 ± 3.4
γS-C_0	0.84 ± 0.15	$(6.2 \pm 1.2) \times 10^6$	−10.3 ± 1.2	−29.8 ± 0.5	−19.5 ± 0.4

https://dx.doi.org/10.1021/acs.biochem.0c00293
Biochemistry 2020, 59, 2371−2385

DTT-resolubilized samples. Notably, γS-C_0 contains a greater proportion of nonmonomeric species. This result is consistent with the extent of structural changes and suggests that both the dimer and high-molecular weight species may be attributable to structural modifications.

To further characterize the EDTA-resolubilized dimers of both proteins, the fractions were collected and subjected to intact protein LC−MS using a C4 UPLC column, as different γ-crystallin conformations have been shown to be separable[90] (Figure 6). Multiple peaks were present in the γS-WT and γS-C_0 traces, allowing us to perform independent mass reconstructions. The major elution peak for both proteins corresponded to an unmodified protein mass. The major peak in both protein traces also contained an earlier-eluting shoulder with an m + 17 mass, likely due to methionine sulfoxide or cysteine sulfenic acid formation, as methionine and cysteine oxidations have previously been reported for γS-crystallin.[35]

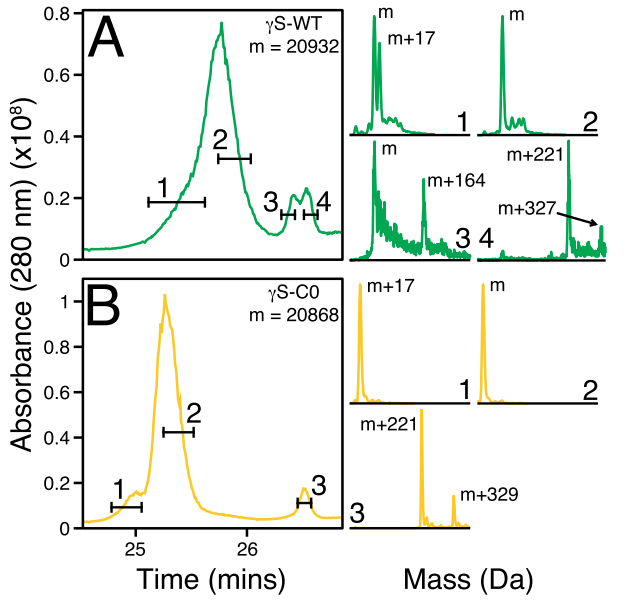

Figure 6. Dimer peaks from chromatographic separation (analytical SEC) of (A) γS-WT and (B) γS-C_0 after EDTA resolubilization were separated on a C4 column prior to mass spectrometry. Two distinct peaks are visible for both proteins, with shouldering or splitting present for most peaks. The selected time frames drawn across the chromatographic traces correspond to the data used for the corresponding mass reconstructions. The fourth selected time frame for γS-WT and the third selected time frame of γS-C_0 correspond to the same chromatographic retention time.

The later-eluting chromatographic peak of γS-WT was split in two. Reconstruction of the earlier peak showed the parent mass and an m + 164 species. The later half of the second peak exhibited masses of m + 221 and m + 327. Likewise, the second peak of γS−C_0, which eluted at the same time as the latter half of the second γS-WT peak, contained an m + 221 peak as well as an m + 329 peak. Although interactions with the column may alter the observed eluted species, the bulk of the eluted protein is copper-free and a minority of protein species have mass shifts indicating the presence of multiple copper ligands. Assuming bound copper and oxidation account for most if not all of the observed mass shifts, an m + 221 species may result from three bound copper ions and two oxidations. Similarly, an m + 331 mass shift resulting from five bound copper ions and a single oxidation is similar to the observed m + 327 and m + 329 mass shifts.

To investigate the contribution of disulfide bonding to copper-induced aggregation, we subjected copper-treated γS-WT peaks from analytical SEC separations to LC−MS using only EDTA, not DTT, prior to chromatographic separation. At only 0.25 equiv of $CuCl_2$, a variety of high-molecular weight species are readily observable and become more pronounced with an increased concentration of $CuCl_2$ (Figure 7A). A substantial recovery of low-molecular weight species is possible via the addition of DTT; however the splitting of the final elution peak that is lost at 1 equiv of $CuCl_2$ cannot be recovered.

Mass reconstructions were used to probe the cause of the splitting observed in the final peak of the analytical SEC chromatograms. Notably, the left and right halves of the final peak contain monomeric and dimeric species (Figure 7B). A −2 Da mass shift occurs in the monomeric species of both final peaks, while a −4 Da mass shift occurs in both peaks' dimeric species. The persistence of the −2 Da mass shift in the monomeric species suggests an intramolecular disulfide bond, while the elimination of the dimeric 2m − 4 peak following DTT treatment suggests the presence of an additional intermolecular disulfide bond. Copper oxidation has been shown to facilitate disulfide bond formation in other γ-crystallins previously,[49,72] and intramolecular disulfide bond formation via the cysteine loop in γS has also been reported.[91]

Mass shifts characteristic of mono- and dioxidation are also present, consistent with intact mass spectrometry of C4-separated dimeric species and previously reported digests.[35] The combination of oxidation and disulfide bond formation accounts for the observed m + 14, m + 30, and 2m + 12 peaks (Figure 7C). The remaining m + 75 and m + 91 monomeric peaks are 61 Da greater than the m + 14 and m + 30 peaks, respectively. This mass difference is consistent with copper binding via bicysteinate coordination. Although it is low in relative abundance, the presence of a 2m + 59 peak also suggests bicysteinate coordination may be responsible for metal-bridged dimerization of two γS-crystallins. This observation is in line with the changes in ITC and tmFRET data at 0.5 equiv of copper. Dimerization via an interface Cu(I) ligand involving a two-coordinate cysteinate-binding site has previously been observed in metalloproteins such as Cox 17,[92] Hah1,[93] yCCS,[94] and Atx1.[95]

Intramolecular Disulfides Are Present in Addition to Bound Copper. To further characterize intramolecular disulfide bond formation and metal binding resulting from copper addition, we turned to native SDS−PAGE. Proteins that remain more compact through conformational trapping[96−98] have been observed to migrate faster through a gel than their native counterparts. Metal binding can also exert a similar effect, whereby the extent of protein unfolding is limited by the geometry of the bound metal.[99] Native SDS−PAGE of $CuCl_2$-treated γS-WT shows four closely spaced bands in the monomeric molecular weight range (Figure 8). The smaller splitting observed between the top and bottom pairs can be attributed to the formation of an intramolecular disulfide (Figures S8 and S9), while the larger splitting of the band pairs results from copper binding. Notably, similar metal gel shifts are also apparent for γD-crystallin when incubated with copper ions.[49−72]

As little as 0.1 equiv of copper is required to observe intramolecular disulfide bond formation and copper binding.

https://dx.doi.org/10.1021/acs.biochem.0c00293
Biochemistry 2020, 59, 2371−2385

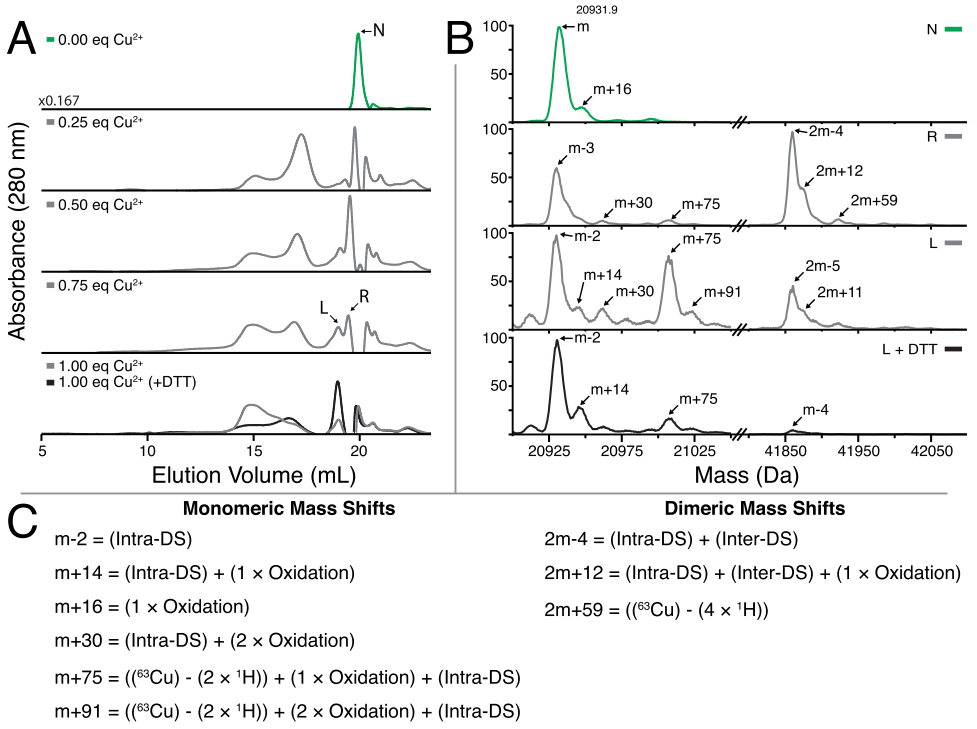

Figure 7. (A) Analytical SEC measurements of γS-WT treated with increasing equivalents of $CuCl_2$ followed by excess EDTA. The addition of $CuCl_2$ results in dimerization of γS-WT, with a shift toward high-molecular weight species with an increase in concentration. Formation of these larger species is partly reversible upon DTT reduction (bottom panel). (B) Protein masses reconstructed using MaxEnt1 for individual peaks collected in panel A. Untreated γS-WT (U) is strictly monomeric, whereas the fractions eluting at the same time (R) and just before (L) the following copper treatment exhibit dimeric character. Reduction via DTT considerably increases the total monomeric content of the L peak. (C) Modifications accounting for the observed mass shifts observed in panel B

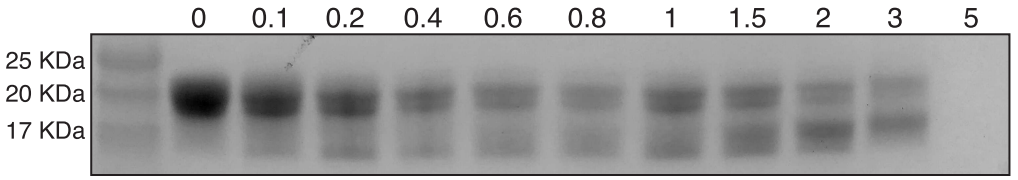

Figure 8. SDS−PAGE analysis of γS-crystallin treated with variable amounts of $CuCl_2$. Soluble γS-WT after incubation with 0, 0.1, 0.2, 0.4, 0.6, 0.8, 1, 1.5, 2, 3, and 5 equiv of $CuCl_2$. Two bands are observed near ∼20 kDa beginning at 0.1 equiv of $CuCl_2$. A lower band below the 17 kDa protein standard is also clearly present after the addition of 0.2 equiv of $CuCl_2$. The lower gel band similarly splits into two close bands with increasing $CuCl_2$ concentrations. The small additional migration within each band pair corresponds to the formation of an intramolecular disulfide bond. The larger additional migration causing the splitting of the band pairs is due to copper binding.

Overloaded SDS−PAGE gels indicate that a small population of dimeric species is also present (Figure S8C). At higher copper:protein ratios, increased amounts of dimer are present, as are gel-shifted dimer bands indicating copper-bound species. Notably absent are any high-molecular weight bands corresponding to large aggregates. Although they are sometimes observed via analytical SEC, intact mass reconstructions show no evidence of species larger than the dimers. In contrast, aggregates of γD-crystallin produced with equivalent amounts of copper do exhibit high-molecular weight species, which are reducible.[49] The SDS−PAGE bands corresponding to copper-bound γS-WT and γS-C_0 are eliminated upon addition of EDTA (Figure S10). The intramolecular disulfide band of γS-WT, however, is not eliminated by addition of either EDTA or DTT.

To narrow down the location of the intramolecular disulfide bond, trypsin digestions were performed on freshly prepared γS-WT that was allowed to incubate with 1 equiv of $CuCl_2$ for 24 h. The resulting peptides were separated and analyzed via liquid chromatography and tandem mass spectrometry (results in Figure 9). The only observable intramolecular disulfide occurred between a peptide fragment containing the cysteine loop and a fragment containing C83. The disulfide bond between the fragments was confirmed through elimination by DTT (RT, 5 min) and isotope pattern analysis. Secondary fragmentation patterns also indicated that the fragments were disulfide-bonded but were insufficient for determining which cysteine was bonded to C83. The structure of the loop region between the second and third β-strands projects the C25 side chain outward (77% solvent-accessible surface area[35]) away from the C83 residue, making this residue unlikely to form the observed intramolecular disulfide without considerable structural rearrangement.[64] A C23−C83 [Protein Data Bank (PDB) entry 6MYG] intramolecular disulfide has been observed in the X-ray crystal structures of mouse γS-crystallins, while a C27−C83 intramolecular disulfide is also plausible as the residues are adjacent to one another in the three-dimensional structure.

https://dx.doi.org/10.1021/acs.biochem.0c00293
Biochemistry 2020, 59, 2371−2385

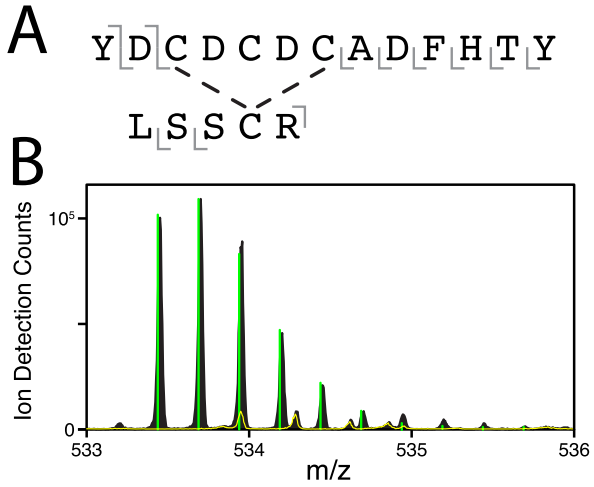

Figure 9. (A) Primary structure of one peptide fragment containing an intramolecular disulfide bond. Gray bars indicate the location of fragmentation observed via MS/MS (detailed in Figures S11 and S12 and Table S1). The location of the disulfide cannot be definitively assigned but is most likely between C83 and either C23 or C27 based on the protein structure. (B) Mass to charge ratio peaks of the parent fragment with (yellow) or without (black) DTT. Green bars represent the predicted isotope pattern of the parent fragment. The elimination of the parent peaks confirms a disulfide linkage.

γS-Crystallin Oxidation May Act as a Buffer against Other Copper-Induced Aggregation Mechanisms. Relative to the α- and β-crystallins, γ-crystallins contain high levels of cysteine (Table S2). At first glance, it appears paradoxical that a protein that is functionally required to maintain a soluble monomeric state over the lifetime of an organism is enriched in this reactive amino acid. However, a high cysteine content can be partially rationalized by this residue's considerable contribution to the protein's refractive index.[35,100] Despite this, the solvent exposure of several γ-crystallin cysteines, particularly those of the cysteine loop, seems incongruent with the importance of resisting oxidation and disulfide bonding in healthy lenses. In aged and cataract lenses, such PTMs have indeed been reported.[16] For γS-crystallin specifically, deamidation and disulfide bonding are particularly common modifications in aged lenses[101,102] and in oxidized samples.[103]

Recently, oxidized γD-crystallin was shown to transfer an intramolecular disulfide bond to the variant γD-W42Q, leading to the hypothesis that intramolecular disulfide bond transfer between γ-crystallins may serve as a final redox buffer for the lens after glutathione depletion.[51] Intermolecular and intramolecular disulfides have also been observed in recent X-ray crystal structures of human and mouse γS-crystallin dimers.[91] Given the high level of solvent exposure of the cysteine loop of human γS, we advance the hypothesis that the tetrad of cysteines in γS acts as a potential oxidation sink of last resort in the lens cortex. Our findings suggest an intramolecular disulfide bond involving C83, which would enable an internal disulfide bond isomerization mechanism for γS (Figure 10). This idea follows from the observation that C83 is buried within γS behind three proximal cysteines. The low abundance of dimeric species across several assays, the observation that γS-crystallin samples stored at higher concentrations for extended periods of time result in more intramolecular than intermolecular disulfides (SI Figure S9), and the previous finding of disulfide bond transfer between γD-crystallins all suggest the hypothesis that γS-crystallin can exchange intermolecular disulfide bonds for intramolecular ones to remain monomeric. Potential intramolecular disulfide bonds and Cu^{2+}-binding sites are shown in Figure 11. Alternatively, an intermolecular disulfide could also function as a lock to prevent unfolding of the native structure, as is observed for the homologous disulfide bond in simulations of γD-crystallin.[104] Further experiments are needed to determine the precise locations of intra- and intermolecular disulfide bonds. However, on the basis of the results available so far, we propose a hypothesis in which the cysteine loop could play a role in the oxidative buffering mechanism, suggesting a purpose for the solvent-accessible cysteines of γS-crystallin beyond their generic role in enhancing refractivity. The proposed ability of the protein to store a disulfide internally is of considerable import given the recent observation that αA-crystallin oxidation reduces stability but enables transfer of a disulfide bond to a substrate protein.[105] Future work will be

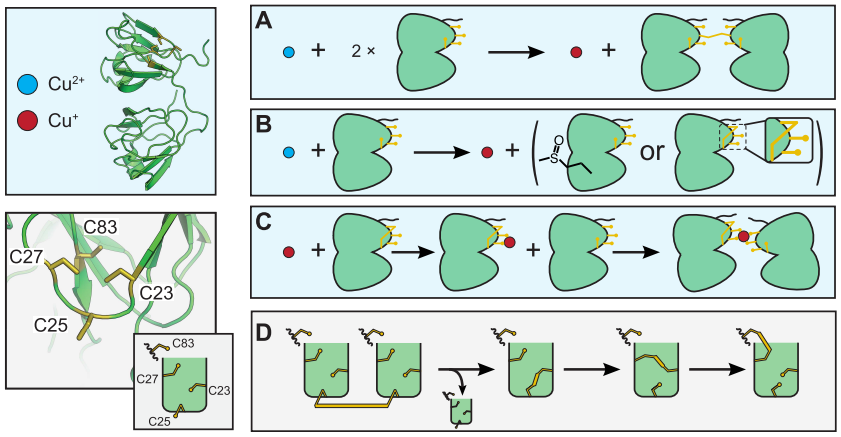

Figure 10. Potential interactions of γS-crystallin involving copper and disulfide bond (gold) transfers. (A) Reduction of Cu(II) to Cu(I) and oxidation of two γS-crystallins resulting in an intermolecular disulfide. (B) Cu(II) is reduced to Cu(I) while γS is oxidized. Oxidation may cause methionine sulfoxide, cysteine sulfenic acid, or intramolecular disulfide bond formation. (C) Binding of Cu(I) to γS-crystallin may lead to the formation of a metal-bridged dimer. (D) Disulfide bond transfer between γS-crystallins most likely involves C25. Although the exact transfer pathway is not yet known, it is clear that C83 is involved in the final intramolecular disulfide. So far, the partner cysteine has not been definitively identified; however, without a large structural rearrangement, C23 and/or C27 must be involved in any intermediary isomerization.

https://dx.doi.org/10.1021/acs.biochem.0c00293
Biochemistry 2020, 59, 2371−2385

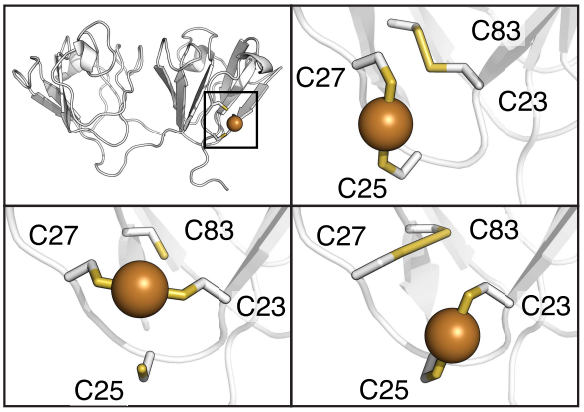

Figure 11. Potential intramolecular disulfide bond and copper-binding site interactions for γS-crystallin. The copper-binding sites shown here involve ligands 180° apart with bond distances of <2.4 Å. (Top left) The bonding interactions are localized to the cysteine loop area of the NTD. (Top right) Potential C23−C83 intramolecular disulfide bond and C25/C27 copper-binding site modeled in γS-crystallin using PDB entry 6MYG.[106] (Bottom right) Alternative possible intramolecular disulfide between C27−C83 and copper-binding sites in γS-crystallin modeled using PDB entry 2M3T.[64] (Bottom left) Copper-binding site in γS-crystallin between C23 and C27 modeled using PDB entry 2M3T.[64]

required to determine whether γS-crystallin can accept a disulfide bond from αA *in vivo* as part of a trade-off between increased αA activity and modification of this structural lens protein.

CONCLUSION

In this study, we observe that the removal of the solvent-accessible cysteines via mutagenesis increases the susceptibility of γS-crystallin to copper-induced aggregation. The reversibility of copper binding to both γS-WT and γS-C_0, which lacks solvent-exposed cysteines, indicates that multiple binding sites are present, raising the possibility that the cysteine tetrad of γS buffers against further aggregation by coordinating to a copper ion. The greater retention of structure of aggregated and soluble γS-WT compared to γS-C_0 also strongly suggests that the cysteine residues are important in buffering unfolding mediated aggregation. Part of the copper buffering capacity of γS-WT is tied to the formation of intramolecular disulfide bonds. The observed intramolecular disulfide involves the buried C83 residue, highlighting the ability of the protein to isomerize a disulfide and also participate in copper binding. The extent to which the intramolecular disulfide may act to alter protein stability is yet unknown. Further experiments will be necessary to determine the additional copper-binding site beyond the cysteine loop and thus refine our understanding of the copper-mediated unfolding mechanisms contributing to aggregation.

ASSOCIATED CONTENT

Supporting Information

The Supporting Information is available free of charge at https://pubs.acs.org/doi/10.1021/acs.biochem.0c00293.

Additional TEM images and characterization data for the γS-crystallin aggregates; FTIR spectra, SEC and SDS−PAGE data, and mass spectrometry data; a figure showing potential ion-binding sites; and tables of literature data for the cysteine content of human crystallin proteins (PDF)

Accession Codes

Human γS-crystallin, Uniprot CRYGS_HUMAN, PDB entries 2M3T and 6FD8; *Mus musculus* (mouse) γS-crystallin, PDB entry 6MY8.

AUTHOR INFORMATION

Corresponding Author

Rachel W. Martin − *Department of Chemistry and Department of Molecular Biology and Biochemistry, University of California, Irvine, California 92697-2025, United States;* orcid.org/0000-0001-9996-7411; Email: rwmartin@uci.edu

Authors

Kyle W. Roskamp − *Department of Chemistry, University of California, Irvine, California 92697-2025, United States*

Sana Azim − *Max Planck Institute for the Structure and Dynamics of Matter, Center for Free Electron Laser Science, Hamburg 22761, Germany*

Günther Kassier − *Max Planck Institute for the Structure and Dynamics of Matter, Center for Free Electron Laser Science, Hamburg 22761, Germany*

Brenna Norton-Baker − *Department of Chemistry, University of California, Irvine, California 92697-2025, United States; Max Planck Institute for the Structure and Dynamics of Matter, Center for Free Electron Laser Science, Hamburg 22761, Germany*

Marc A. Sprague-Piercy − *Department of Molecular Biology and Biochemistry, University of California, Irvine, California 92697-3900, United States*

R. J. Dwyane Miller − *Max Planck Institute for the Structure and Dynamics of Matter, Center for Free Electron Laser Science, Hamburg 22761, Germany; Departments of Chemistry and Physics, University of Toronto, Toronto, ON M5S 3H6, Canada;* orcid.org/0000-0003-0884-0541

Complete contact information is available at: https://pubs.acs.org/10.1021/acs.biochem.0c00293

Funding

This work was supported by National Institutes of Health Grants 2R01EY021514 to R.W.M. and 1R01EY025328 to R.W.M. and D. J. Tobias. K.W.R. was supported by National Science Foundation (NSF) Training Grant DGE-1633631 and grant DMS-1361425 to R.W.M. and C. T. Butts. B.N.-B. was supported by the NSF GRFP and the Fulbright Fellowship. M.A.S.-P. was supported by the Howard Hughes Medical Institute Gilliam Fellowship. R.J.D.M. acknowledges the Max Planck Society and the Excellence Cluster "The Hamburg Center for Ultrafast Imaging (CUI)-Structure, Dynamics and Control of Matter at the Atomic Scale" of the Deutsche Forschungsgemeinschaft (DFG). R.W.M. and R.J.D.M. are CIFAR Fellows.

Notes

The authors declare no competing financial interest.

ACKNOWLEDGMENTS

The authors acknowledge Dmitry Fishman for assistance and management of optical instruments at the UCI Laser Spectroscopy Labs, Ben Katz and Felix Grun for extensive help with mass spectrometry data analysis and management of the UCI Mass Spectrometry Facility, Friedjof Tellkamp,

Hendrik Schikora, and Martin Kollewe from the machine physics support group, and Djordje Gitaric and Josef Gonschior from the technical staff of the Max Planck Institute for the Structure and Dynamics of Matter for setting up the UVB source. This work builds on discussions at the 2018 Crystallin Satellite Biophysical Society Meeting in San Francisco, and we are grateful to the participants for ideas and suggestions.

REFERENCES

(1) Fagerholm, P. P., Philipson, B. T., and Lindström, B. (1981) Normal human lens - the distri- bution of protein. *Exp. Eye Res. 33*, 615−620.
(2) Serebryany, E., and King, J. A. (2014) The $\beta\,\gamma$-crystallins: Native state stability and pathways to aggregation. *Prog. Biophys. Mol. Biol. 115*, 32−41.
(3) Vendra, V. P. R., Khan, I., Chandani, S., Muniyandi, A., and Balasubramanian, D. (2016) Gamma crystallins of the human eye lens. *Biochim. Biophys. Acta, Gen. Subj. 1860*, 333−343.
(4) Serebryany, E., Razban, R., and Shakhnovich, E. I. (2019) Conformational catalysis of cataract-associated aggregation by interacting intermediates in a human eye lens Crystallin. *arXiv*, 1904.03653.
(5) Horwitz, J., Bova, M. P., Ding, L.-L., Haley, D. A., and Stewart, P. L. (1999) Lens α- Crystallin: function and structure. *Eye 13*, 403−408.
(6) Stengel, F., Baldwin, A. J., Painter, A. J., Jaya, N., Basha, E., Kay, L. E., Vierling, E., Robin- son, C. V., and Benesch, J. L. P. (2010) Quaternary dynamics and plasticity underlie small heat shock protein chaperone function. *Proc. Natl. Acad. Sci. U. S. A. 107*, 2007−2012.
(7) Chen, J., Flaugh, S. L., Callis, P. R., and King, J. (2006) Mechanism of the highly effi- cient quenching of tryptophan fluorescence in human γD-Crystallin. *Biochemistry 45*, 11552−11563.
(8) Chen, J., Toptygin, D., Brand, L., and King, J. (2008) Mechanism of the efficient trypto- phan fluorescence quenching in human γD-Crystallin studied by time-resolved fluorescence. *Biochemistry 47*, 10705−10721.
(9) Chen, J., Callis, P. R., and King, J. (2009) Mechanism of the very efficient quenching of tryptophan fluorescence in human γD-and γS-crystallins: the γ-Crystallin fold may have evolved to protect tryptophan residues from ultraviolet photodamage. *Biochemistry 48*, 3708−3716.
(10) King, J., Mills Henry, I., Kosinski-Collins, M., Thol, S., and Serebryany, E. (2020) Buried tryptophans contributing to the high kinetic stability of the long-lived gamma crystallins and their oxidative damage opening the pathway to the aggregated state associated with cataracts. *Biophys. J. 118*, 181A.
(11) Schafheimer, N., and King, J. (2013) Tryptophan cluster protects human γD-Crystallin from ultraviolet radiation-induced photoaggregation in vitro. *Photochem. Photobiol. 89*, 1106−1115.
(12) Bova, L., Wood, A., Jamie, J., and Truscott, R. (1999) UV filter compounds in human lenses: The origin of 4-(2-amino-3-hydroxyphenyl)-4-oxobutanoic acid O-beta-D-glucoside. *Invest. Ophthalmol. Visual Sci. 40*, 3237−3244.
(13) Parker, N. R., Jamie, J. F., Davies, M. J., and Truscott, R. J. W. (2004) Protein-bound kynurenine is a photosensitizer of oxidative damage. *Free Radical Biol. Med. 37*, 1479−1489.
(14) Serebryany, E., Takata, T., Erickson, E., Schafheimer, N., Wang, Y., and King, J. A. (2016) Aggregation of Trp>Glu point mutants of human γD-Crystallin provides a model for heredi- tary or UV-induced cataract. *Protein Sci. 25*, 1115−1128.
(15) Giblin, F. J. (2000) Glutathione: a vital lens antioxidant. *J. Ocul. Pharmacol. Ther. 16*, 121−135.
(16) Hains, P. G., and Truscott, R. J. (2007) Post-translational modifications in the nuclear region of young, aged, and cataract human lenses. *Journal of Proteome Res. 6*, 3935−3943.
(17) Wilmarth, P., Tanner, S., Dasari, S., Nagalla, S., Riviere, M., Bafna, V., Pevzner, P., and David, L. (2006) Age-related changes in human crystallins determined from comparative analysis of post-translational modifications in young and aged lens: does deamidation con- tribute to Crystallin insolubility? *Journal of Proteome Res. 5*, 2554−2566.
(18) Lampi, K. J., Wilmarth, P. A., Murray, M. R., and David, L. L. (2014) Lens β -crystallins: the role of deamidation and related modifications in aging and cataract. *Prog. Biophys. Mol. Biol. 115*, 21−31.
(19) Harrington, V., McCall, S., Huynh, S., Srivastava, K., and Srivastava, O. P. (2004) Crystallins in water soluble-high molecular weight protein fractions and water insoluble protein fractions in aging and cataractous human lenses. *Mol. Vision 10*, 476−489.
(20) Lampi, K. J., Ma, Z., Hanson, S. R., Azuma, M., Shih, M., Shearer, T. R., Smith, D. L., Smith, J. B., and David, L. L. (1998) Age-related changes in human lens crystallins identified by two-dimensional electrophoresis and mass spectrometry. *Exp. Eye Res. 67*, 31−43.
(21) Forsythe, H. M., Vetter, C. J., Jara, K. A., Reardon, P. N., David, L. L., Barbar, E. J., and Lampi, K. J. (2019) Altered protein dynamics and increased aggregation of human γS-Crystallin due to cataract-associated deamidations. *Biochemistry 58*, 4112−4124.
(22) Vetter, C. J., Thorn, D. C., Wheeler, S. G., Mundorff, C., Halverson, K., Carver, J. A., David, L. L., and Lampi, K. J. (2020) Accumulative deamidation of human lens protein γS-Crystallin leads to partially unfolded intermediates with enhanced aggregation propensity. *bioRxiv*, DOI: 10.1101/2020.02.21.960237.
(23) Fujii, N., Momose, Y., Ishibashi, Y., Uemura, T., Takita, M., and Takehana, M. (1997) Specific racemization and isomerization of the aspartyl residue of αA-Crystallin due to UV-B irradiation. *Exp. Eye Res. 65*, 99−104.
(24) Hooi, M. Y. S., Raftery, M. J., and Truscott, R. J. W. (2012) Racemization of two proteins over our lifespan: deamidation of asparagine 76 in γS Crystallin is greater in cataract than in normal lenses across the age range. *Invest. Ophthalmol. Visual Sci. 53*, 3554−3561.
(25) Hains, P. G., and Truscott, R. J. (2008) Proteomic analysis of the oxidation of cysteine residues in human age-related nuclear cataract lenses. *Biochim. Biophys. Acta, Proteins Proteomics 1784*, 1959−1964.
(26) Linetsky, M., and Ortwerth, B. (1997) Quantitation of the singlet oxygen produced by UVA irradiation of human lens proteins. *Photochem. Photobiol. 65*, 522−529.
(27) Zigman, S. (1995) Environmental near-UV radiation and cataracts. *Optom. and Vis. Sci. 72*, 899−901.
(28) Ghosh, K. S., Pande, A., and Pande, J. (2011) Binding of γ-Crystallin substrate prevents the binding of copper and zinc ions to the molecular chaperone α-Crystallin. *Biochemistry 50*, 3279−3281.
(29) Cekic, O. (1998) Effect of cigarette smoking on copper, lead, and cadmium accumulation in human lens. *Br. J. Ophthalmol. 82*, 186−188.
(30) Balaji, M., Sasikala, K., and Ravindran, T. (1992) Copper levels in human mixed, nuclear brunescence, and posterior subcapsular cataract. *Br. J. Ophthalmol. 76*, 668−669.
(31) Rácz, P., and Ördögh, M. (1977) Investigations on trace elements in normal and senile cataractous lenses. *Albrecht von Graefes Arch. Klin. Exp. Ophthalmol. 204*, 67−72.
(32) Aydin, E., Cumurcu, T., Özuğurlu, F., Özyurt, H., Sahinoglu, S., Mendil, D., and Hasdemir, E. (2005) Levels of iron, zinc, and copper in aqueous humor, lens, and serum in nondiabetic and diabetic patients. *Biol. Trace Elem. Res. 108*, 033−042.
(33) Ahmad, A., Ahmad, I., Khan, M. A., Munshi, A. B., Siddiqui, I., Anzar, O., and Anzar, A. (2014) On-set of cataract and accumulation of copper, lead and cadmium in smokers of Karachi. *Journal of Environmental & Analytical Toxicology 5*, 2.
(34) Langford-Smith, A., Tilakaratna, V., Lythgoe, P. R., Clark, S. J., Bishop, P. N., and Day, A. J. (2016) Age and smoking related changes in metal ion levels in human lens: implications for cataract formation. *PLoS One 11*, No. e0147576.

(35) Roskamp, K. W., Kozlyuk, N., Sengupta, S., Bierma, J. C., and Martin, R. W. (2019) Divalent cations and the divergence of $\beta\ \gamma$-Crystallin function. *Biochemistry 58*, 4505−4518.
(36) Tabner, B. J., Turnbull, S., El-Aganf, O., and Allsop, D. (2001) Production of reactive oxygen species from aggregating proteins implicated in Alzheimer's disease, Parkinson's disease and other neurodegenerative diseases. *Curr. Top. Med. Chem. 1*, 507−517.
(37) Manoharan, S., Guillemin, G. J., Abiramasundari, R. S., Essa, M. M., Akbar, M., and Akbar, M. D. (2016) The role of reactive oxygen species in the pathogenesis of Alzheimer's dis- ease, Parkinson's disease, and Huntington's disease: a mini review. *Oxid. Med. Cell. Longevity 2016*, 8590578.
(38) Binolfi, A., Quintanar, L., Bertoncini, C. W., Griesinger, C., and Fernández, C. O. (2012) Bioinorganic chemistry of copper coordination to alpha-synuclein: Relevance to Parkinson's disease. *Coord. Chem. Rev. 256*, 2188−2201.
(39) Wang, X., Moualla, D., Wright, J. A., and Brown, D. R. (2010) Copper binding regulates intracellular alpha-synuclein localisation, aggregation and toxicity. *J. Neurochem. 113*, 704−714.
(40) Bush, A. I. (2003) The metallobiology of Alzheimer's disease. *Trends Neurosci. 26*, 207−214.
(41) Faller, P., Hureau, C., and La Penna, G. (2014) Metal ions and intrinsically disordered pro- teins and peptides: from Cu/Zn amyloid-β to general principles. *Acc. Chem. Res. 47*, 2252−2259.
(42) Arnesano, F., Scintilla, S., Calò, V., Bonfrate, E., Ingrosso, C., Losacco, M., Pellegrino, T., Rizzarelli, E., and Natile, G. (2009) Copper-triggered aggregation of ubiquitin. *PLoS One 4*, No. e7052.
(43) Bocharova, O. V., Breydo, L., Salnikov, V. V., and Baskakov, I. V. (2005) Copper (II) inhibits in vitro conversion of prion protein into amyloid fibrils. *Biochemistry 44*, 6776−6787.
(44) Zhou, L.-X., Du, J.-T., Zeng, Z.-Y., Wu, W.-H., Zhao, Y.-F., Kanazawa, K., Ishizuka, Y., Nemoto, T., Nakanishi, H., and Li, Y.-M. (2007) Copper (II) modulates in vitro aggregation of a tau peptide. *Peptides 28*, 2229−2234.
(45) Wang, X., Garcia, C. M., Shui, Y.-B., and Beebe, D. C. (2004) Expression and regulation of α-, β -, and γ-crystallins in mammalian lens epithelial cells. *Invest. Ophthalmol. Visual Sci. 45*, 3608−3619.
(46) Robinson, N. E., Lampi, K. J., Speir, J. P., Kruppa, G., Easterling, M., and Robinson, A. B. (2006) Quantitative measurement of young human eye lens crystallins by direct injection Fourier transform ion cyclotron resonance mass spectrometry. *Mol. Vision 12*, 704−711.
(47) Siezen, R. J., Thomson, J. A., Kaplan, E. D., and Benedek, G. B. (1987) Human lens gamma- crystallins: isolation, identification, and characterization of the expressed gene products. *Proc. Natl. Acad. Sci. U. S. A. 84*, 6088−6092.
(48) Konz, I., Fernández, B., Fernández, M. L., Pereiro, R., González-Iglesias, H., Coca-Prados, M., and Sanz-Medel, A. (2014) Quantitative bioimaging of trace elements in the human lens by LA-ICP-MS. *Anal. Bioanal. Chem. 406*, 2343−2348.
(49) Quintanar, L., Domínguez-Calva, J., Serebryany, E., Rivillas-Acevedo, L., Haase-Pettingell, C., Amero, C., and King, J. (2016) Copper and zinc ions specifically promote nonamyloid aggregation of the highly stable human γD-Crystallin. *ACS Chem. Biol. 11*, 263−272.
(50) Bloemendal, H., de Jong, W., Jaenicke, R., Lubsen, N. H., Slingsby, C., and Tardieu, A. (2004) Ageing and vision: structure, stability and function of lens crystallins. *Prog. Biophys. Mol. Biol. 86*, 407−485.
(51) Serebryany, E., Yu, S., Trauger, S. A., Budnik, B., and Shakhnovich, E. I. (2018) Dynamic disulfide exchange in a Crystallin protein in the human eye lens promotes cataract-associated aggregation. *J. Biol. Chem. 293*, 17997−18009.
(52) Sweeney, M. H., and Truscott, R. J. (1998) An impediment to glutathione diffusion in older normal human lenses: A possible precondition for nuclear cataract. *Exp. Eye Res. 67*, 587−595.
(53) Studier, F. W. (2005) Protein production by auto-induction in high-density shaking cultures. *Protein Expression Purif. 41*, 207−234.
(54) Roskamp, K. W., Montelongo, D. M., Anorma, C. D., Bandak, D. N., Chua, J. A., Malecha, K. T., and Martin, R. W. (2017) Multiple aggregation pathways in human γS- xrystallin and Its aggregation-prone G18V variant. *Invest. Ophthalmol. Visual Sci. 58*, 2397−2405.
(55) Khago, D., Wong, E. K., Kingsley, C. N., Alfredo Freites, J., Tobias, D. J., and Martin, R. W. (2016) Increased hydrophobic surface exposure in the cataract-related G18V variant of hu- man γS-Crystallin. *Biochim. Biophys. Acta, Gen. Subj. 1860*, 325−332.
(56) R Core Team (2015) *R: A Language and Environment for Statistical Computing*, R Foundation for Statistical Computing, Vienna.
(57) Liu, Y. (2016) *Package 'Ritc': Isothermal Titration Calorimetry (ITC) Data Analysis*, Johns Hopkins University, Baltimore.
(58) Eftink, M., and Selvidge, L. (1982) Fluorescence quenching of liver alcohol dehydrogenase by acrylamide. *Biochemistry 21*, 117−125.
(59) Gordon, S. E., Senning, E. N., Aman, T. K., and Zagotta, W. N. (2016) Transition metal ion FRET to measure short-range distances at the intracellular surface of the plasma membrane. *J. Gen. Physiol. 147*, 189−200.
(60) Pande, A., Annunziata, O., Asherie, N., Ogun, O., Benedek, G. B., and Pande, J. (2005) Decrease in protein solubility and cataract formation caused by the Pro23 to Thr mutation in human γD-Crystallin. *Biochemistry 44*, 2491−2500.
(61) Boatz, J. C., Whitley, M. J., Li, M., Gronenborn, A. M., and van der Wel, P. C. (2017) Cataract-associated P23T γD-Crystallin retains a native-like fold in amorphous-looking ag- gregates formed at physiological pH. *Nat. Commun. 8*, 15137.
(62) Karri, S., Kasetti, R. B., Vendra, V. P. R., Chandani, S., and Balasubramanian, D. (2013) Structural analysis of the mutant protein D26G of human γS-Crystallin, associated with Cop- pock cataract. *Mol. Vision 19*, 1231−1237.
(63) Bharat, S. V., Shekhtman, A., and Pande, J. (2014) The cataract-associated V41M mutant of human γS-Crystallin shows specific structural changes that directly enhance local surface hydrophobicity. *Biochem. Biophys. Res. Commun. 443*, 110−114.
(64) Brubaker, W. D., and Martin, R. W. (2012) 1 H, 13 C, and 15 N assignments of wild-type human γS-Crystallin and its cataract-related variant γS-G18V. *Biomol. NMR Assignments 6*, 63−67.
(65) Haris, P. I., and Severcan, F. (1999) FTIR spectroscopic characterization of protein structure in aqueous and non-aqueous media. *J. Mol. Catal. B: Enzym. 7*, 207−221.
(66) Fatima, U., Sharma, S., and Guptasarma, P. (2010) Structures of differently aggregated and precipitated forms of γB Crystallin: An FTIR spectroscopic and EM study. *Protein Pept. Lett. 17*, 1155−1162.
(67) Vendra, V. P. R., Chandani, S., and Balasubramanian, D. (2012) The mutation V42M dis- torts the compact packing of the human gamma-S-Crystallin molecule, resulting in congenital cataract. *PLoS One 7*, No. e51401.
(68) Ji, F., Jung, J., Koharudin, L. M., and Gronenborn, A. M. (2013) The human W42R γD- Crystallin mutant structure provides a link between congenital and age-related cataracts. *J. Biol. Chem. 288*, 99−109.
(69) Talla, V., Narayanan, C., Srinivasan, N., and Balasubramanian, D. (2006) Mutation causing self-aggregation in human γC-Crystallin leading to congenital cataract. *Invest. Ophthalmol. Visual Sci. 47*, 5212−5217.
(70) Matulis, D., Baumann, C. G., Bloomfield, V. A., and Lovrien, R. E. (1999) 1-Anilino-8- naphthalene sulfonate as a protein conformational tightening agent. *Biopolymers 49*, 451−458.
(71) Kim, I., Saito, T., Fujii, N., Kanamoto, T., Chatake, T., and Fujii, N. (2015) Site specific oxidation of amino acid residues in rat lens γ-Crystallin induced by low-dose γ-irradiation. *Biochem. Biophys. Res. Commun. 466*, 622−628.
(72) Ramkumar, S., Fan, X., Wang, B., Yang, S., and Monnier, V. M. (2018) Reactive cysteine residues in the oxidative dimerization and Cu2+ induced aggregation of human γD-Crystallin: Implications for age-related cataract. *Biochim. Biophys. Acta, Mol. Basis Dis. 1864*, 3595−3604.
(73) Domínguez-Calva, J. A., Haase-Pettingell, C., Serebryany, E., King, J. A., and Quintanar, L. (2018) A histidine switch for Zn-induced aggregation of γ-crystallins reveals a metal- bridging

https://dx.doi.org/10.1021/acs.biochem.0c00293
Biochemistry 2020, 59, 2371−2385

mechanism that Is relevant to cataract disease. *Biochemistry 57*, 4959−4962.
(74) Domínguez-Calva, J., Pérez-Vázquez, M., Serebryany, E., King, J., and Quintanar, L. (2018) Mercury-induced aggregation of human lens γ-crystallins reveals a potential role in cataract disease. *JBIC, J. Biol. Inorg. Chem. 23*, 1105−1118.
(75) Smith, R., Martell, A., and Motekaitis, R. (2004) NIST standard reference database 46. National Institute of Standards and Technology.
(76) Xiao, Z., Brose, J., Schimo, S., Ackland, S. M., La Fontaine, S., and Wedd, A. G. (2011) Unification of the copper (I) binding affinities of the metallo-chaperones Atx1, Atox1, and related proteins: Detection probes and affinity standards. *J. Biol. Chem. 286*, 11047−11055.
(77) Krężel, A., Leśniak, W., Jeżowska-Bojczuk, M., Młynarz, P., Brasuñ, J., Kozłowski, H., and Bal, W. (2001) Coordination of heavy metals by dithiothreitol, a commonly used thiol group protectant. *J. Inorg. Biochem. 84*, 77−88.
(78) Flaugh, S. L., Kosinski-Collins, M. S., and King, J. (2005) Contributions of hydrophobic domain interface interactions to the folding and stability of human γD-Crystallin. *Protein Sci. 14*, 569−581.
(79) Kosinski-Collins, M. S., Flaugh, S. L., and King, J. (2004) Probing folding and fluorescence quenching in human γD Crystallin Greek key domains using triple tryptophan mutant pro- teins. *Protein Sci. 13*, 2223−2235.
(80) Ma, Z., Piszczek, G., Wingfield, P. T., Sergeev, Y. V., and Hejtmancik, J. F. (2009) The G18V CRYGS mutation associated with human cataracts increases γS-Crystallin sensitivity to thermal and chemical stress. *Biochemistry 48*, 7334−7341.
(81) Moreau, K. L., and King, J. (2009) Hydrophobic core mutations associated with cataract development in mice destabilize human γD-Crystallin. *J. Biol. Chem. 284*, 33285−33295.
(82) Whitley, M. J., Xi, Z., Bartko, J. C., Jensen, M. R., Blackledge, M., and Gronenborn, A. M. (2017) A combined NMR and SAXS analysis of the partially folded cataract-associated V75D γD-Crystallin. *Biophys. J. 112*, 1135−1146.
(83) Changela, A., Chen, K., Xue, Y., Holschen, J., Outten, C. E., O'Halloran, T. V., and Mon- dragón, A. (2003) Molecular basis of metal-ion selectivity and zeptomolar sensitivity by CueR. *Science 301*, 1383−1387.
(84) Lu, C.-H., Lin, Y.-F., Lin, J.-J., and Yu, C.-S. (2012) Prediction of metal ion−binding sites in proteins using the fragment transformation method. *PLoS One 7*, No. e39252.
(85) Lin, Y.-F., Cheng, C.-W., Shih, C.-S., Hwang, J.-K., Yu, C.-S., and Lu, C.-H. (2016) MIB: metal ion-binding site prediction and docking server. *J. Chem. Inf. Model. 56*, 2287−2291.
(86) Brose, J., La Fontaine, S., Wedd, A. G., and Xiao, Z. (2014) Redox sulfur chemistry of the copper chaperone Atox1 is regulated by the enzyme glutaredoxin 1, the reduction potential of the glutathione couple GSSG/2GSH and the availability of Cu (I). *Metallomics 6*, 793−808.
(87) Zimmermann, M., Clarke, O., Gulbis, J. M., Keizer, D. W., Jarvis, R. S., Cobbett, C. S., Hinds, M. G., Xiao, Z., and Wedd, A. G. (2009) Metal binding affinities of Arabidopsis zinc and copper transporters: selectivities match the relative, but not the absolute, affinities of their amino-terminal domains. *Biochemistry 48*, 11640−11654.
(88) North, M. L., and Wilcox, D. E. (2019) Shift from entropic Cu^{2+} binding to enthalpic Cu^{+} binding determines the reduction thermodynamics of blue copper proteins. *J. Am. Chem. Soc. 141*, 14329−14339.
(89) Kanwar, R., and Balasubramanian, D. (1999) Structure and stability of the dityrosine-linked dimer of γB-Crystallin. *Exp. Eye Res. 68*, 773−784.
(90) Buhr, F., Jha, S., Thommen, M., Mittelstaet, J., Kutz, F., Schwalbe, H., Rodnina, M. V., and Komar, A. A. (2016) Synonymous codons direct cotranslational folding toward different protein conformations. *Mol. Cell 61*, 341−351.
(91) Thorn, D. C., Grosas, A. B., Mabbitt, P. D., Ray, N. J., Jackson, C. J., and Carver, J. A. (2019) The structure and stability of the disulfide-linked γS-Crystallin dimer provide insight into oxidation products associated with lens cataract formation. *J. Mol. Biol. 431*, 483−497.
(92) Abajian, C., Yatsunyk, L. A., Ramirez, B. E., and Rosenzweig, A. C. (2004) Yeast Cox17 solution structure and copper (I) binding. *J. Biol. Chem. 279*, 53584−53592.
(93) Wernimont, A. K., Huffman, D. L., Lamb, A. L., O'Halloran, T. V., and Rosenzweig, A. C. (2000) Structural basis for copper transfer by the metallochaperone for the Menkes/Wilson disease proteins. *Nat. Struct. Biol. 7*, 766−771.
(94) Rosenzweig, A. C., and O'Halloran, T. V. (2000) Structure and chemistry of the copper chap- erone proteins. *Curr. Opin. Chem. Biol. 4*, 140−147.
(95) Banci, L., Bertini, I., Cantini, F., Felli, I. C., Gonnelli, L., Hadjiliadis, N., Pierattelli, R., Rosato, A., and Voulgaris, P. (2006) The Atx1-Ccc2 complex is a metal-mediated protein- protein interaction. *Nat. Chem. Biol. 2*, 367−368.
(96) Fountoulakis, M., Juranville, J.-F., Stüber, D., Weibel, E. K., and Garotta, G. (1990) Pu- rification and biochemical characterization of a soluble human interferon gamma receptor expressed in *Escherichia coli*. *J. Biol. Chem. 265*, 13268−13275.
(97) Taniyama, Y., Kuroki, R., Omura, F., Seko, C., and Kikuchi, M. (1991) Evidence for in- tramolecular disulfide bond shuffling in the folding of mutant human lysozyme. *J. Biol. Chem. 266*, 6456−6461.
(98) Chen, W., Li, L., Du, Z., Liu, J., Reitter, J. N., Mills, K. V., Linhardt, R. J., and Wang, C. (2012) Intramolecular disulfide bond between catalytic cysteines in an intein precursor. *J. Am. Chem. Soc. 134*, 2500−2503.
(99) Shelake, R. M., Ito, Y., Masumoto, J., Morita, E. H., and Hayashi, H. (2017) A novel mech- anism of 'metal gel-shift' by histidine-rich Ni^{2+}-binding Hpn protein from *Helicobacter py- lori* strain SS1. *PLoS One 12*, No. e0172182.
(100) Khago, D., Bierma, J. C., Roskamp, K. W., Kozlyuk, N., and Martin, R. W. (2018) Protein refractive index increment is determined by conformation as well as composition. *J. Phys.: Condens. Matter 30*, 435101.
(101) Ma, Z., Hanson, S. R., Lampi, K. J., David, L. L., Smith, D. L., and Smith, J. B. (1998) Age-related changes in human lens crystallins identified by HPLC and mass spectrometry. *Exp. Eye Res. 67*, 21−30.
(102) Hanson, S. R., Smith, D. L., and Smith, J. B. (1998) Deamidation and disulfide bonding in human lens γ-crystallins. *Exp. Eye Res. 67*, 301−312.
(103) Skouri-Panet, F., Bonneté, F., Prat, K., Bateman, O. A., Lubsen, N. H., and Tardieu, A. (2001) Lens crystallins and oxidation: the special case of γS. *Biophys. Chem. 89*, 65−76.
(104) Serebryany, E., Woodard, J. C., Adkar, B. V., Shabab, M., King, J. A., and Shakhnovich, E. I. (2016) An internal disulfide locks a misfolded aggregation-prone intermediate in cataract- linked mutants of human γD-Crystallin. *J. Biol. Chem. 291*, 19172−19183.
(105) Kaiser, C. J., Peters, C., Schmid, P. W., Stavropoulou, M., Zou, J., Dahiya, V., Mym- rikov, E. V., Rockel, B., Asami, S., Haslbeck, M., Rappsilber, J., Reif, B., Zacharias, M., Buchner, J., and Weinkauf, S. (2019) The structure and oxidation of the eye lens chaperone αA-Crystallin. *Nat. Struct. Mol. Biol. 26*, 1141−1150.
(106) Sagar, V., and Wistow, G. (2018) Mouse γS-Crystallin L16 octamer. To be published.

https://dx.doi.org/10.1021/acs.biochem.0c00293
Biochemistry 2020, 59, 2371−2385